Coculture model of a liver sinusoidal endothelial cell barrier and HepG2/C3a spheroids-on-chip in an advanced fluidic platform

Taha Messelmani, Anne Le Goff, Fabrice Soncin, Zied Souguir, Franck Merlier, Nathalie Maubon, Cécile Legallais, Eric Leclerc, Rachid Jellali

Coculture model of a liver sinusoidal endothelial cell barrier and HepG2/C3a spheroids-on-chip in an advanced fluidic platform

Taha Messelmani [1], Anne Le Goff [1], Fabrice Soncin [2,3], Zied Souguir [4], Franck Merlier [5], Nathalie Maubon [4], Cécile Legallais [1], Eric Leclerc [1,3], Rachid Jellali[1]*

[1] *Université de Technologie de Compiègne, CNRS, Biomechanics and Bioengineering, Centre de recherche Royallieu-CS 60319 -60203 Compiègne Cedex, France*

[2] *CNRS/IIS/Centre Oscar Lambret/Lille University SMMiL-E Project, CNRS Délégation Hauts-de-France, 43 Avenue le Corbusier, 59800 Lille, France*

[3] *CNRS, IRL2820, Laboratory for Integrated Micro Mechatronic Systems, Institute of Industrial Science, University of Tokyo, 4-6-1 Komaba, Meguro-ku, Tokyo 153-8505, Japan*

[4] *HCS Pharma, 250 rue Salvador Allende, Biocentre Fleming Bâtiment A, 59120 Loos, France*

[5] *Université de Technologie de Compiègne, UPJV, CNRS, Enzyme and Cell Engineering, Centre de Recherche Royallieu, Cedex CS 60319, 60203 Compiègne, France*

Corresponding authors: Rachid Jellali (rachid.jellali@utc.fr)

ABSTRACT

The liver is one of the main organs involved in the metabolism of xenobiotics and a key organ in toxicity studies. Prior to accessing the hepatocytes, xenobiotics pass through the hepatic sinusoid formed by liver sinusoidal endothelial cells (LSECs). The LSECs barrier regulates the kinetics and concentrations of the xenobiotics before their metabolic processing by the hepatocytes. To mimic this physiological situation, we developed an *in vitro* model reproducing an LSECs barrier in coculture with a hepatocyte biochip, using a fluidic platform. This technology made dynamic coculture and tissue crosstalk possible. SK-HEP-1 and HepG2/C3a cells were used as LSECs and as hepatocyte models, respectively. We confirmed the LSECs phenotype by measuring PECAM-1 and stabilin-2 expression levels and the barrier's permeability/transport properties with various molecules. The tightness of the SK-HEP-1 barrier was enhanced in the dynamic coculture. The morphology, albumin secretion, and gene expression levels of markers of HepG2/C3a were not modified by coculture with the LSECs barrier. Using paracetamol, a well-known hepatotoxic drug, to study tissue crosstalk, there was a reduction in the expression levels of the LSECs markers stabilin-2 and PECAM-1, and a modification of those of CLEC4M and KDR. No HepG2/C3a toxicity was observed. The metabolisation of paracetamol by HepG2/C3a monocultures and cocultures was confirmed. Although primary cells are required to propose a fully relevant model, the present approach highlights the potential of our system for investigating xenobiotic metabolism and toxicity.

Keywords: Organ-on-chip, Liver, LSECs barrier, HepG2/C3a, coculture, microfluidic

INTRODUCTION

Animal models are widely used as reference tools for predictive studies in drug development and risk assessment **(1)**. However, due to differences between animal and human metabolism and physiology, animal models fail to accurately reproduce the human condition, and this issue challenges the extrapolation of data to humans **(2,3)**. For example, the predictivity of animal models for chemical-induced hepatotoxicity is only 50% **(4)**. Moreover, animal experiments are costly, time-consuming and most importantly raise ethical and regulatory issues **(4,5)**. To decrease the use of animals, the REACH legislation and the 3R rules, recommended to reduce as much as possible the use of animal models, have pressed industrial companies and scientists to develop alternative approaches to animal testing **(2)**. Consequently, developing reliable methods not based on *in vivo* experimentation has become necessary.

The liver is the main site involved in the metabolism of xenobiotics and is therefore the most commonly used organ in toxicological and pharmacological tests **(6,7)**. It is composed of several cell types, the main ones being hepatocytes (parenchymal cells) and non-parenchymal cells (NPCs): sinusoidal endothelial cells (LSECs), Kupffer cells (KCs), hepatic stellate cells (HSCs), and biliary epithelial cells **(8,9)**. Hepatocytes represent approximately 60% of the total liver cells, and are the main cell type, ensuring most metabolic activities **(10)**. The NPCs are involved in several key functions, such as the production of growth factors and mediators of cellular functions, maintenance of tissue architecture, and regulation of liver response to xenobiotics **(8,9)**.

Currently, most of the *in vitro* liver models are focused on hepatocytes and do not include NPCs **(11)**. Moreover, the models used for drug screening and risk assessment are mainly based on cell culture in static two-dimension (2D) monolayers **(1)**. These 2D cultures present some advantages, such as allowing high throughput analyses, ease of manipulation, and a lower cost **(9,12)**. However, 2D monocultures of hepatocytes or of hepatic cell lines suffer from several

disadvantages associated with the loss of tissue-specific architecture, mechanical and biomechanical cues, and cell-cell and cell-matrix interactions. Consequently, these models fail to recapitulate the complexity of the *in vivo* physiological environment, show limited prediction capacity for xenobiotics, and cells are prone to dedifferentiation within 48-72 h **(1,12,13)**.

Recently, several approaches have been proposed to overcome the drawbacks associated with 2D monolayer cultures of hepatocytes. Microfluidic devices, or organ-on-chip (OoC) technology, are a promising tool for building more relevant *in vitro* liver models aimed at mimicking the *in vivo* environment **(14)**. The microfluidic perfusion improves the exchanges and transport of nutrients, oxygen, and other chemicals, and creates a controlled micro-environment and physiological-like features, including the liver zonation, cell-cell interactions, shear stress, and chemical concentration gradients **(1,9,15,16)**. Several studies have reported that perfused microfluidic cultures enhance the long-term viability and functionality of hepatocytes **(17-19)**. The three-dimensional (3D) cell culture (spheroids/organoids), with and without polymer matrix, also makes it possible to maintain tissue architecture similar to the *in vivo* situation and maintains liver-specific functions. This organisation enhances cell-cell and cell-matrix interactions and the creation of chemical gradients **(6,20,21)**. Among other approaches used to maintain hepatocyte functions, cocultures with NPCs are commonly used strategies **(4)**. Among NPCs, LSECs participate in liver metabolic functions and maintain hepatocyte phenotype and functions through paracrine communication **(22)**. The benefits of coculturing LSECs and hepatocytes have been reported in several works **(22-24)**.

Previously, we developed a liver-on-chip model integrating a hydroscaffold containing key liver extracellular matrix (ECM) components **(25).** This device made possible the dynamic culture of HepG2/C3a organised into 3D spheroids for the long-term, while maintaining their functionalities. Here, to better reproduce the physiology of the liver, our HepG2/C3a-on-chip model was cocultured with LSECs. The coculture was performed using a fluidic platform

previously developed by our laboratory **(26)** making it possible to connect the biochip to a new LSEC barrier insert. The behaviour and functionalities of the LSECs barrier (SK-HEP-1 cell line) and hepatocyte biochip (HepG2/C3a cells) in monoculture and coculture were studied and compared. Then, the coculture model was exposed to paracetamol (APAP), and the crosstalk between both compartments was studied and compared to monocultures exposed to APAP.

MATERIALS AND METHODS

Manufacturing of the biochip

The biochip fabrication and design were described in our previous work **(27)**. The biochip consists of two polydimethylsiloxane (PDMS) layers (Sylgard 184 kit; Dow Corning, Midland, TX, USA)) manufactured by soft lithography and sealed via air plasma treatment (Harrick Scientific, Ithaca, NY, USA). The microstructured bottom layer contains chambers and microchannels (height of 100 µm), and the top layer, with a 100 µm-deep reservoir, includes an inlet and outlet for culture medium perfusion (**Fig.S1A**).

To promote 3D cell organisation, the BIOMIMESYS® Liver hydroscaffold (HCS Pharma, Loos, France) was integrated into the biochip. BIOMIMESYS® Liver is a hyaluronic acid (HA)-based hydroscaffold composed of RGDS-grafted HA, galactosamine-grafted HA, collagen type I and collagen type IV. The hydroscaffold preparation was performed in accordance with a previously patented process **(28)**. Briefly, the pseudo-hydrogel solution (HA, collagen and crosslinker: adipic acid dihydrazide) was injected into the biochip and the hydroscaffold crosslinking was performed *in situ*. The biochips were then washed, freeze-dried, and sterilised using ultraviolet (UV) exposure. The detailed characterization of the biochips (with and without hydroscaffold) was reported in our previous work **(25)**. The pictures and microscope images of the biochips with and without hydroscaffolds are presented in **Fig.S1B and C**.

Coculture platform: IIDMP fluidic device

We used the previously described Integrated Insert in a Dynamic Microfluidic Platform (IIDMP, **26**) coculture system which consists of a polycarbonate platform with three subunits (**Fig.1A** and **Fig.S2**). Each subunit is composed of the association of an insert and a biochip linking two wells. The insert was placed in the first well and defined an apical pole (LSECs barrier) and a basal pole making possible the exchange of culture medium between the LSECs barrier and the hepatocyte compartment (biochip, **Fig.1A**). The biochip connected the first and second well (acting as a reservoir). The volume of culture medium was 10 mL: 1 mL placed in the apical insert, 5 mL below the insert, and 4 ml in the second well. Culture medium flowed through the biochip from the basal compartment in the first well towards the second well. The perfusion fluid was provided by a cover connected to a peristaltic pump (Ismatec™, Wertheim, Germany) via PTFE (polytetrafluoroethylene) tubing. The other components of the IIDMP platform were silicone gaskets sealing the device, and a bottom layer composed of the well subunits, thanks to which the biochips were connected (at the bottom, **Fig.S2**).

Cells and culture media

HepG2/C3A, a clone of the HepG2 line derived from human hepatocellular carcinoma (ATCC CRL-10741; LGC Standards, Molsheim, France), were used as the hepatocyte model. They were cultured in Minimal Essential Medium (MEM) with phenol red (Pan Biotech, Aidenbach, Germany), 10% fetal bovine serum (FBS; Gibco,Waltham, MA,USA), 1 mM hydroxy-ethylpiperazine-N-2-ethanesulfonic acid (HEPES, Gibco), 2 mM L-glutamine (Gibco), 0.1 mM non-essential amino acids (Gibco), 1 mM sodium pyruvate (Gibco), and 100 U/mL penicillin, 100 µg/mL streptomycin (Pan Biotech). The SK-HEP-1 cell line (ATCC HTB-52; LGC Standards) derived from an adenocarcinoma of the liver was used as the LSECs model. For maintenance, SK-HEP-1 cells were cultured in a mixture of 75% EGM-2 medium (Lonza, Verviers, Belgium) and 25% MEM (complemented as mentioned above).

All cells were cultured in 75 cm^2 flasks at 37°C in a humidified atmosphere with 5% of CO_2. The culture medium was renewed every 2 days and the cells were passaged weekly (confluence of 80-90%). To decrease variability, the cells were used between passages 10-20.

Optimisation of common culture medium for HepG2/C3A and SK-HEP-1 cells

Culture medium optimisation was performed in static conditions, and different MEM/EGM-2 ratios were tested. The SK-HEP-1 cells were seeded in cell culture inserts (THINCERT, 6-well format, polyethylene terephthalate membrane, 0.4 µm pore; Greiner Bio-One, Les Ulis, France) at a density of 0.35 x 10^5 cell/cm^2. The culture medium was renewed every 2 days in the apical (1 mL) and basal (2 mL) compartments, and the culture was maintained until confluence was attained (6-8 days). The HepG2/C3A were seeded in the wells of a 6-well plate (Greiner Bio-One) at a density of 1 x 10^5 cell/cm^2. The culture was maintained for 4 days, and the medium (2 mL) was changed every 2 days. The cultures were continuously maintained at 37°C in a 5% CO_2 supplied incubator and the assays were performed at the end of the experiments.

Dynamic monoculture and coculture in the IIDMP device

Each experiment lasted two days (**Fig.1B**). The SK-HEP-1 inserts were maintained for 8 days for the formation of a confluent barrier, before performing the dynamic experiments, as mentioned in section 2.4.1. In parallel, 24 h before the dynamic experiments, HepG2/C3a cells were seeded in the biochips containing the hydroscaffold (4 x 10^5 cell/biochip), and the biochips were incubated overnight at 37°C in a humidified atmosphere with 5% of CO_2.

On Day 0 of the experiment, the SK-HEP-1 previously grown for 8 days on inserts were transferred into the first well of the IIDMP device and the HepG2/C3a biochips were connected to the bottom of the device. As shown in **Fig.1B**, three conditions were established: SK-HEP-1 monoculture (IIDMP with insert alone), HepG2/C3a monoculture (IIDMP with biochip alone) and coculture (IIDMP containing insert and biochip). Culture medium was added (1 mL in the

apical insert side, 5 mL in the basal side and 4 mL in the reservoir well), the IIDMP was closed and connected to the pump. The entire setup was placed in the incubator and perfusion started at 10 µL/min for 48 h in a closed loop. For exposure to drugs, acetaminophen (APAP; Sigma-Aldrich, Saint-Quentin-Fallavier, France) was loaded into the apical compartment of the insert at 1 mM before perfusion started (an insert without cells was used for HepG2/C3a monoculture experiments). After dilution in the total medium in the circuit (10 mL), the systemic concentration of APAP was 100 µM.

Lucifer Yellow permeability assay

Lucifer Yellow (LY CH dipotassium salt, Sigma-Aldrich) was diluted in Hanks' balanced salt solution (HBSS, with $CaCl_2$ and $MgCl_2$, Gibco) at 50 µM and loaded into the apical compartment of an empty insert and inserts with cells were cultured for 4-15 days. The basal compartment was filled with HBSS. The inserts were then incubated at 37°C and 5% of CO_2. After 90 min, medium from the apical and basal compartments was collected. The fluorescence intensity was measured using a Spectafluor Plus microplate reader (TECAN, Männedorf, Switzerland) at excitation/emission wavelengths of 485/530 nm. The flow of LY was expressed by the calculation of the apparent permeability (Papp, m/s) as follows: **Papp = (dQ/dt) x (1/AxCa),** where dQ/dt is the amount of LY transported during a given time (mol/s), Ca is the initial concentration of LY solution (mol/m^3) and A is the surface of the insert (m^2).

Permeability to dextrans

The SK-HEP-1 barrier's permeability to molecules of different molecular weights was assessed using fluorescein isothiocyanate-dextrans (FITC-dextran 4, 70 and 150 kDa, Sigma-Aldrich). The assays were performed using confluent SK-HEP-1 barriers (8 days of culture) in static and dynamic (IIDMP device) conditions. The dextrans were diluted in the culture medium at a concentration of 100 µg/mL and deposited in the apical compartment of the culture inserts. Then, culture medium was sampled in the apical and basal compartments at different times. The

FITC-dextran fluorescence intensity was measured using a Spectafluor Plus microplate reader (TECAN) at excitation/emission wavelengths of 490/525 nm.

Immunostaining assays

Immunostaining assays were performed using fixed and permeabilised SK-HEP-1 inserts. The samples were incubated overnight with primary antibodies, then for 12 h with the secondary antibodies (4°C in the dark). The primary and secondary antibodies used were mouse anti-CD31 (1 µg/mL; ab24590, Abcam, Cambridge, UK), rabbit anti-stabilin-2 (1 µg/mL; ab121893, Abcam), mouse anti-vimentin (1 µg/mL; ab8978, Abcam), donkey anti-mouse Alexa Fluor 647 (2 µg/mL; ab150107, Abcam) and goat anti-rabbit Alexa Fluor 488 (2 µg/mL; A11034, Invitrogen, Waltham, MA, USA). Actin filaments were stained with Alexa Fluo 488 Phalloidin for 3h (1/50; Thermo Fisher Scientific, Illkirch, France). Nuclei were stained with 10 µg/mL 4′,6-diamidino-2-phenylindole (DAPI, D1306, Invitrogen) for 30 min at room temperature in the dark. Imaging was obtained with a laser scanning confocal microscope (LSM 710; Zeiss, Oberkochen, Germany).

Albumin, interleukin-6 and urea measurements

ELISA sandwich assays were used to quantify the albumin and IL-6 concentrations in the culture media collected at the end of the experiments. The assays were performed using a human albumin ELISA Quantitation Set (E80-129; Bethyl Laboratories, Montgomery, TX, USA) and a human IL-6 ELISA Kit (ab718013; Abcam) for albumin and IL-6, respectively, following the protocols recommended by the manufacturers. The urea was quantified using a QuantiChrom urea assay kit (DIUR-100; BioAssay Systems, Hayward, CA, USA). The kit contains a chromogenic reagent that forms a colored complex specifically with urea. The results were acquired using a Spectafluor Plus microplate reader (TECAN) set to a wavelength of 450 nm (albumin and IL-6) and 520 nm (urea).

225 **RNA extraction and RTqPCR analysis**

226 At the end of the experiments, the cells were lysed and recovered using 500 µL of TRIzol
227 (Thermo Fischer Scientific). Total RNA was purified by phenol/chloroform extraction followed
228 by alcohol precipitation, and RNA concentrations measured using a NanodropOne (Thermo
229 Fisher Scientific). Reverse transcription reactions were performed using a High-capacity cDNA
230 reverse transcription kit with RNase inhibitor (Applied Biosystems, ThermoFisher Scientific).
231 Quantitative PCRs were performed using a StepOnePlus machine (Applied Biosystems,
232 Thermo Fisher Scientific) in duplex reactions, mixing the cDNA with the TaqMan FAM-
233 labelled probes of the analyzed gene (Applied Biosystems, Thermo Fisher Scientific) and with
234 β2-microglobulin-VIC-labeled probe in the same reaction well (**Table S1**). The threshold cycle
235 (C_T) values were calculated at the upper linear range of the logarithm^{-2} amplification curve
236 using the StepOne v2.3 software (Thermo Fisher scientific). The data were then expressed as
237 $2^{-\Delta\Delta C_T}$. ΔC_T is the difference between the C_T of the analyzed gene and the C_T of the β2-
238 microglobulin gene used as normalizer in the same reaction. $\Delta\Delta C_T$ is the difference between
239 the mean ΔC_T of the experimental samples and the mean ΔC_T of the control samples **(29)**. The
240 relative quantity (RQ) corresponds to $2^{-\Delta\Delta C_T}$ which transforms the logarithmic^{-2} data into
241 decimal values.

242 **HPLC-HRMS**

243 Detection and quantitative evaluation of APAP and APAP metabolites was performed
244 with high performance liquid chromatography coupled to high resolution mass spectrometry
245 (HPLC-HRMS). The HPLC system (Infinity 1290; Agilent Technologies, Les Ulis, France)
246 with DAD, was connected to a Q-TOF micro hybrid quadrupole time of flight mass
247 spectrometer (Agilent 6538; Agilent Technologies) with electrospray ionisation (ESI). HPLC
248 was carried out on a Thermo Hypersyl Gold C18 (USP L1) column (150 × 4.6 mm ID, 5 µm,
249 175 A), connected to the Agilent Infinity 1290 HPLC at 40°C.

Statistical analysis

All experiments were performed at least three times and a minimum of 2 bio-chips/inserts/cocultures were performed in each experiment (N = 3 experiments and n = 6). Data are presented as means ± standard deviations (SD) of the 6 replicates (for RTqPCR assays, only 3 replicates from 3 different experiments were used). To determine statistical differences, a one-way ANOVA (Kruskal-Wallis test, multiple groups) and unpaired t-test (two groups) were performed using GraphPad Prism 8.4.3 software (San Diego, CA, USA). Data with P values < 0.05 were identified as statistically significant and highlighted in the figures.

RESULTS

Selecting a culture medium for SK-HEP-1 and HepG2/C3a coculture

The culture of cells of different origin in the same system requires an adapted coculture medium capable of maintaining both cell types in good conditions, without impairing their characteristics and functionalities. The routine culture medium used in our conditions for SK-HEP-1 is EGM-2/MEM (75%/25%) and the cells formed a well-structured cell monolayer at confluence, as needed for the barrier function (**Fig.2A** and **S3**). On the other hand, when SK-HEP-1 cells were cultured in HepG2/C3a medium, which is based on MEM only, the endothelial cell morphology was greatly altered, and the cells failed to form a confluent monolayer (**Fig.S3**). In an attempt to, first, create the endothelial barrier, and then to switch to a hepatocyte culture medium, SK-HEP-1 cells were cultured in their normal medium for 6 days, followed by culture in MEM for 3 days (as the coculture period). In these conditions again, the endothelial cells failed to maintain a confluent monolayer (**Fig.S3**). In both conditions (MEM and EGM-2/MEM (75%/25%) followed by MEM), a large number of rounded cells in suspension was observed, suggesting that cells failed to attach or attached but exhibited poor adhesion. Finally, when cells were maintained in EGM-2/MEM (25%/75%) medium for 7 days, the SK-HEP-1 cells formed a confluent monolayer (**Fig.2A** and **S3**) and exhibited the

characteristic morphology of SK-HEP-1, as when cultured in their original medium. The gene expression levels of several LSECs markers were investigated. No major differences were observed for most of the genes when cells were cultured in EGM-2/MEM (25%/75%) when compared to their original medium. A downregulation of CLEC4M and VCAM1 was observed when cells were maintained in EGM-2/MEM (25%/75%) in comparison with native medium, with fold changes (FC) of 0.25 and 0.48, respectively (**Fig.2B**).

The EGM-2/MEM (25%/75%) medium was also tested on HepG2/C3a cells and compared to culturing in MEM. After 4 days of static culture, the HepG2/C3a presented a typical morphology and formed a monolayer in both conditions (**Fig.2C**). Additionally, secretion of albumin was measured to assess whether HepG2/C3a cells retained their hepatic properties. Similar albumin secretion levels were observed in both conditions. The levels were approximately 125 ± 11 and 114 ± 17 ng/h for cells cultured in MEM and EGM-2/MEM 1/3 mixture, respectively (**Fig.2D**). Based on the results obtained with SK-HEP-1 and HepG2/C3a cells, the mixture of EGM-2/MEM (25%/75%) was chosen for the dynamic coculture experiments. To facilitate the comparisons between monoculture and coculture, this medium was also used for SK-HEP-1 and HepG2/C3a maintenance in monocultures.

Characterisation of the SK-HEP-1 endothelial barrier

LSECs act as a physical barrier to molecules and play a significant role in transportation from circulating blood to the hepatocytes. Therefore, before using SK-HEP-1 to form a liver endothelial barrier in our coculture model, it was essential to characterise the formation, integrity, and permeability of the barrier. The SK-HEP-1 cells were seeded in static inserts using the selected coculture medium and followed over time. The cells proliferated continuously to reach full confluence and form homogenous and continuous monolayers from Days 7-8 and thereafter (**Fig.S4**). Then, overgrowth could be observed, resulting in the formation of a second layer of cells on top of the first one (Day 10, **Fig.S4**). Nevertheless, the

formation of continuous layers of confluent cells was confirmed by nuclei, vimentin, and actin stainings. As shown in **Fig.3A**, the tissue was dense with contiguous cells and a well-developed actin network. The LSECs phenotype of the SK-HEP-1 barrier was confirmed by the positive staining for LSECs markers PECAM-1 and stabilin-2 (**Fig.3B**).

The formation of a confluent barrier was associated with major modifications in paracellular permeability. The flow through the barrier was directly correlated to the integrity and homogeneity of the barrier. To confirm the formation of the barrier, permeability to Lucifer Yellow was checked using SK-HEP-1 inserts at different times of culture. PET inserts without cells exhibited a permeability value of $177 \times 10^{-15} \pm 9 \times 10^{-15}$ m/s (**Fig.3C**). When SK-HEP-1 cells were added, a significant decrease in Lucifer Yellow paracellular flow from the apical to the basal compartment was observed, with apparent permeability values of $98 \times 10^{-15} \pm 10 \times 10^{-15}$ and $35 \times 10^{-15} \pm 1 \times 10^{-15}$ m/s at Days 4 and 8, respectively. This latter value remained stable, at approximately $40 \times 10^{-15} \pm 8 \times 10^{-15}$ m/s until Day 15. These results suggested that the SK-HEP-1 cells were capable of forming a barrier which reached relative stability at Day 8, and could be used for coculture with HepG2/C3a and permeability experiments.

The permeability of the SK-HEP-1 barrier to molecules with different molecular weights was also assessed, using FITC-dextran of 4, 70 and 150 kDa. The experiments were performed using confluent SK-HEP-1 cultures at Day 8 in static inserts. For comparison, the same experiments were performed using inserts without cells. When using each of the different molecular weight dextrans, we found that the tracer concentrations decreased from the apical compartment and increased in the basal one over time (**Fig.3D**). Thus, the tracer molecules were able to pass through the insert membranes whether the cells were present or not. However, the FITC dextrans diffused at faster rates into the basal compartment when the inserts were not seeded with endothelial cells, whereas the presence of a SK-HEP-1 cell layer slowed the diffusion process for the three molecular weight markers, confirming that the SK-HEP-1 made

an efficient diffusion barrier. As expected, the diffusion rates were dependent on the FITC-dextran molecular weight and were slower when using FITC-dextran of 150 kDa when compared to 4 kDa- dextran.

Effect of the dynamic coculture on the SK-HEP-1 barrier

Following the previous characterisations and optimisations, the coculture of SK-HEP-1 barrier (LSECs compartment) with HepG2/C3a cells cultured in 3D in the biochip (the hepatocyte compartment as previously characterised **(25)**) was assessed. The coculture was performed for 48 h in the IIDMP platform and the communication between both compartments was ensured by culture medium circulation. In parallel, for comparison, SK-HEP-1 and HepG2/C3a monocultures were also used in the IIDMP platform.

After 8 days of barrier maturation in static conditions followed by 48 h of dynamic coculture or monoculture, the SK-HEP-1 inserts were collected and characterised. Although cells were barely distinguishable because of the density at confluence, the morphology of the SK-HEP-1 tissues appeared similar in coculture and monoculture. In both culture modes, the cells formed homogenous and continuous barriers and grew beyond confluence (**Fig.S5**). Confocal microscopy imaging of actin, vimentin and nuclei staining confirmed the formation of a continuous endothelial barrier, with different cell layers and a developed actin/vimentin network (**Fig.4A**). Furthermore, no obvious differences were observed between the staining of cocultured and monocultured barriers. SK-HEP-1 barriers in monoculture and coculture expressed typical LSECs markers without any apparent difference between the two modes of culture, as illustrated by the detection of PECAM-1 and stabilin-2 positive cells (**Fig.4B**).

Gene expression level analyses of several LSECs markers revealed the significant upregulation of CLEC4M (FC: 2.05) whereas KDR was downregulated (FC: 0.49) in SK-HEP-1 cocultures (**Fig.5A**). The expression levels of PECAM-1, MRC1 and CD32b were similar in SK-HEP-1 monocultures and cocultures. Finally, the diffusion of FITC-dextran 4 kDa through

the barrier, in dynamic monoculture and coculture with HepG2/C3a, were compared. The results in **Fig.5B** confirmed the permeability of the barrier and the communication between the apical and basal side, in both culture conditions. The variations in FITC-dextran concentrations in the apical compartment revealed a lower diffusion rate through the barrier in coculture when compared to that in monoculture, notably after 24 h.

Behaviour and functionality of HepG2/C3a in coculture with the SK-HEP-1 barrier

The day before starting the dynamic monocultures/cocultures in the IIDMP device, HepG2/C3a cells were seeded into the biochips containing the hydroscaffold and incubated in static conditions (adhesion phase). After 24 h, the cells were embedded in/adhered to the hydroscaffold and started to create spheroid-like aggregates (**Fig.6A**). Then, the biochips were connected to the IIDMP device, with and without an SK-HEP-1 barrier, and perfusion was started. The cells maintained in coculture with an endothelial barrier had a similar morphology to cells maintained in monoculture. In both conditions, the HepG2/C3a formed a dense tissue, organised in 3D spheroids ranging between 200 and 500 µm in diameter (**Fig.6A**). To evaluate the effects of coculture on the specific functions of HepG2/C3a, albumin and urea secretions were quantified. Albumin levels in coculture were found to be similar to those in monoculture (**Fig.6B**). After 48 h of culture, the albumin secretion was 127 ± 24 and 134 ± 28 ng/h in monoculture and coculture, respectively. Regarding urea, the secretion was higher in HepG2/C3a monoculture (2.34 ± 0.28 µg/h), than in coculture (1.50 ± 0.31 µg/h, **Fig.6C**). Finally, the expression of several specific genes of HepG2/C3a cells (UGT2B7, UGT1A1, SULT1A2, CYP1A2 and CYP1A1) were also evaluated. As shown in **Fig.6D**, there were no significant differences in expression levels in the selected genes between HepG2/C3a maintained as a monoculture and HepG2/C3a in coculture with SK-HEP-1.

Exposure of the coculture and monoculture models to acetaminophen (APAP)

To test the coculture model and demonstrate the crosstalk between the HepG2/C3a biochips and SK-HEP-1 barrier in the configuration of a drug study, we exposed the SK-HEP-1/HepG2/C3a coculture to APAP and compared the results with SK-HEP-1 and HepG2/C3amonocultures. APAP was chosen because it is i) metabolised by HepG2/C3a cells, ii) widely studied with liver *in vitro* models, and iii) not adsorbed by the PDMS biochip **(30)**. APAP was introduced into the apical side of the SK-HEP-1 barrier at 1 mM, leading to a systemic theorical concentration of 100 µM after diffusion in the total circuit. For comparative purposes, HepG2/C3a monoculture in the IIDMP was also performed and APAP was deposited into the insert without SK-HEP-1.

SK-HEP-1 cells exposed to APAP for 48 h in coculture or in monoculture exhibited a confluent and continuous barrier composed of several cell layers, forming a dense tissue. The cell morphologies between the treated SK-HEP-1 barrier in coculture and in monoculture showed no significant differences (**Fig.S6**). Moreover, the SK-HEP-1 cells exposed to APAP were similar to those without APAP (monoculture and coculture, **Fig.S5**). As shown in **Fig.7A** and **S7**, APAP treatment appeared to affect the actin cytoskeleton of the barrier, both in monoculture and coculture. In the cultures without APAP, the actin filaments appear to be organized and localized around the nuclei (**Fig.4A** and **S7**). Conversely, with APAP exposure (**Fig.7A** and **S7**), this organization around the nuclei is not observable and the actin filaments appear disordered and composed of more elongated filaments. The immunostaining of specific LSECs markers showed weaker expression levels of PECAM-1 and stabilin-2 in SK-HEP-1 exposed to APAP (**Fig.7B**), when compared to monoculture and coculture without APAP (**Fig.4B**). This effect was more striking in the coculture. Gene expression analyses of cultures treated or not with APAP showed an upregulation of KDR (FC: 1.8) after APAP exposure in coculture (**Fig.8A**). Conversely, both this gene and CLEC4M were downregulated in the

monoculture exposed to APAP (FC: 0.54 and 0.49 for CLEC4M and KDR, respectively). APAP treatment of the monoculture also led to the upregulation of MRC1 (FC 1.4).

Regarding the HepG2/C3a biochip, the cells exposed to APAP (coculture or monoculture) maintained their organisation in 3D spheroids up until the end of the culture (**Fig.S6**). The cells formed dense tissues, without any apparent difference compared to non-treated cultures. Analysis of gene expression showed no differences between the biochip monocultures treated or not with APAP (**Fig.8B**). For HepG2/C3a cocultured with the SK-HEP-1 barrier, UGT2B7 expression levels were downregulated (FC: 0.7). In both monoculture and coculture, the albumin secretion was not affected by APAP treatment. The ratios of albumin secretion (culture with APAP versus without APAP) were 0.92 ± 0.25 and 0.95 ± 0.09 for monoculture and coculture, respectively (**Fig.8C**). Conversely, the APAP treatment was associated with a 2.4- and 1.6-fold reduction in urea secretion for monoculture and coculture, respectively (**Fig.8C**).

The metabolism of APAP was then investigated in cocultures and monocultures using HPLC-HRMS. We used the basal culture medium to confirm the passage of APAP through the SK-HEP-1 barrier. The ratios of APAP (compared to the initial systemic concentration of 100 µM) recovered at the end of the experiment are provided in **Fig.8D**. For the SK-HEP-1 monoculture, the APAP ratio at the end of the experiment was 1.02 ± 0.07, indicating that SK-HEP-1 did not metabolise APAP. The recovered ratio, corresponding to a concentration of 100 µM, confirmed the passage of APAP through the barrier, allowing the equilibrium of APAP concentration between the apical and basal sides. In the HepG2/C3a monoculture and SK-HEP-1/HepG2/C3a coculture, the APAP ratios were 0.83 ± 0.05 and 0.87 ± 0.08, respectively, illustrating metabolism (**Fig.8D**). However, for both conditions, the paracetamol sulphate and paracetamol glucuronide concentrations were below detection limits.

Expression of inflammatory cytokines

The expression of inflammatory cytokines was evaluated in all cultures (with and without APAP) by analysing mRNA levels for TNFα, IL-1, IL-6 and IL-8 genes, and by quantifying IL-6 secretion. SK-HEP-1 cells expressed the four genes in all culture conditions (monoculture/coculture and APAP+/APAP-). Gene expression levels of IL8, IL6 and IL1 were similar, regardless of the culture conditions. There was a noticeable significant upregulation of TNFα in SK-HEP-1 cocultured with APAP (**Fig.8E**). Regarding HepG2C3a cells, there were no significant differences in expression levels of IL-8 in the conditions tested. On the other hand, there was a slight but significant overexpression of TNFα in HepG2/C3a cocultured without APAP when compared to monocultures (**Fig.8F**). IL-6 protein quantification in culture medium showed that it was only expressed by SK-HEP-1 cells and that HepG2/C3a monocultures with and without APAP did not produce detectable amounts of IL-6 (**Fig.8G**).

DISCUSSION

Classic 2D *in vitro* coculture models consist of cells randomly mixed and heterogeneously distributed at the bottom of well-plates and dishes. However, *in vivo,* LSECs and hepatocytes are separated by the space of Disse which, in 3D models, is generally mimicked by a gel or collagen matrix which physically separates LSECs and hepatocytes **(23)**. Furthermore, controlling the homotypic and heterotypic cell-to-cell interactions appears to be a key feature for maintaining and enhancing the hepatocyte phenotype **(31,32)**. In the present work, we have established a coculture model of liver sinusoidal endothelial cells with liver cell line. Thanks to our platform which integrates a liver-on-chip solution and a barrier insert, we were able to propose technology that physically separated both cell types. In this model, cell-to-cell paracrine-like communication was made possible by exchanges through the insert membrane, as this model did not allow direct contact between LSECs and hepatocytes. Although this type of technology has already been presented for organ-to-organ models such as the intestine

barrier-liver **(26)**, to our knowledge, only a few other dynamic LSECs barrier-hepatocyte coculture models have previously been described **(33-35)**.

We demonstrated the functionality of the coculture model using two human cell lines, SK-HEP-1 and HepG2/C3a. For this purpose, we optimised the culture medium, confirmed the innocuity of the fluid flow and coculture on the LSECs barriers, and characterised the cytokine crosstalk between cells. Establishing a coculture medium that is healthy for two or more types of cells is a critical step in *in vitro* physiological models **(36)**, including liver cells **(34)**. Similarly, it was reported that LSECs are sensitive to serum components **(37)**. Our data demonstrated that the HepG2/C3a MEM-based medium which contained serum contributed to damaging the LSECs layer, whereas the conventional LSECs medium (also containing serum) did not. Interestingly, a mixture of the HepG2/C3a and SK-HEP-1 media led to both healthy LSECs and HepG2/C3a. Although we did not identify the specific factors leading to this result, we postulate that the presence of pro-angiogenic factors in EGM-2 medium played a part in stabilising the LSEC cultures. Interestingly, the present dynamic conditions did not affect the cell junctions or the expression levels of LSEC markers.

Endothelial cells are normally exposed to flow, and dynamic *in vitro* models have largely been reported as regulating their functions and physiology **(38,39)**. However, a decrease in endothelial barrier permeability was only reported in dynamic cultures coupled to high shear stress (0.7-1 Pa) **(39)**. In the present work, we did not observe significant variations in barrier permeability functions between static and dynamic SK-HEP-1 monocultures (**Fig.3D** and **5B**). Indeed, in the IIDMP device, the flow passes in the basal side and the SK-HEP-1 cells (facing the apical side) are not directly exposed to the shear. Conversely, the permeability was reduced in dynamic LSECs cocultures (**Fig.5B**), illustrating stronger cell junctions in the presence of HepG2/C3a, and suggesting that there is a synergistic effect of cells coculture in our conditions. We also measured that CLEC4M, an important LSECs marker **(40)** was overexpressed in

coculture. Furthermore, we found that the LSECs produced basal levels of pro-inflammatory cytokines IL6 and TNF without any significant morphology damage. The dynamic coculture also did not play a part in significantly increasing cytokine levels in LSECs. As high levels of pro-inflammatory cytokines production in the liver by LSECs leads to fibrosis **(41)**, our result illustrated the fact that the dynamic cocultures of LSECs were not pro-inflammatory.

Previous works reported an improved hepatocyte phenotype when cocultured with endothelial cells **(22-24,42)**. In the present model, we did not detect any striking benefit of the presence of LSECs on the HepG2/C3a phenotype (no albumin increase, no mRNA gene metabolism upregulation, no clear cytokine over secretion). In fact, the enhanced maturation of hepatocytes was mainly reported on primary hepatocytes that tend to rapidly dedifferentiate **(42)**. It is clear that the hepatocarcinoma HepG2/C3a cell line is probably not an ideal model for liver-on-chip approaches. Although it has been widely used in works related to cancer and liver disease **(43)**, and shown that interactions between the liver endothelium (include SK-HEP-1) and this liver carcinoma were reported in studies investigating liver disorders **(44,45)**, it has a weak maturation profile. It is certainly a robust model for proof-of-principle studies, but the present on-chip approach would clearly benefit from being extended and refined using normal human primary cells.

Regarding liver toxicology, the liver's *in vivo* features suggest that xenobiotics must first pass the endothelial barrier before accessing the hepatocytes. Analysing the kinetics and toxicity of APAP *via* the LSEC barrier and its subsequent metabolism inside the HepG2/C3a compartment was presented as a proof of concept of our technology. APAP was selected because its metabolism and effect with HepG2/C3a cells have been widely studied, including in our biochip **(46-49)**. Although HepG2/C3a do not express the CYP2E1, they highly express CYP1A2 (involved in the APAP metabolism, **(50)**) in our biochip **(48)**. To ensure healthy and functional cells, low concentration of APAP (100 µM) was used. APAP toxicity directly on

LSECs has already been reported in the literature **(51,52)**. The presence of APAP contributed to modifying the expression of LSECs markers in this work. This was illustrated by degradation of the actin and vimentin network, and the reduction of the PECAM-1 and STAB2 expression levels as shown in the immunostaining images. We also confirmed APAP metabolism in the presence of the HepG2/C3a cells. The barrier led to modulation of the concentration of APAP reaching the liver cells and we did not detect any particular sign of HepG2/C3a toxicity in our experiments. Consistently with the literature, the 100 µM concentration of APAP on HepG2 is not a toxic concentration, as most studies reported effects between 1 to 2 mM **(49,53,54)**.

The development of relevant *in vitro* liver models is very challenging. With the progress made in tissue engineering and microfluidics, several microfluidic-based models reproducing a physiologically relevant microenvironment have been developed in recent years **(9,16)**. Although most of these models are based on hepatocyte monoculture, a growing number of groups are interested in developing microfluidic cocultures of different liver cells, especially hepatocytes and LSECs **(9,16,22,35,55,56)**. In these models, the different cell types are randomly mixed or organised in layers separated by a porous membrane, collagen layer or microstructures **(16,23)**. The present model combines the advantages of the LSECs barrier and hepatocytes cultured in 3D spheroids in hyaluronic acid hydroscaffold. Thanks to the IIDMP platform, the LSEC insert and the hepatocytes biochips are physically separated to mimic the space of Disse which separates both cells *in vivo*. The interaction between LSECs and HepG2/C3a is ensured only *via* the paracrine communication. A critical issue in microfluidic culture is the balance between model relevance, complexity and practicality. For liver cell cocultures, all cell types are usually seeded in the same irreversibly sealed microfluidic device, which makes it extremely difficult to analyse the different cell types separately **(57)**. Our model consists of two separate compartments easily assembled in the IIDMP devices: HepG2/C3a in biochips and the LSECs barrier in standard inserts. Each cell type can be cultured and

characterised separately before being connected to an IIDMP device for coculture. At the end of the experiments, the inserts and biochips can also be easily removed for separate external analyses.

Overall, the present study provides an original model based on coculture of HepG2/C3a spheroids-on-chip with LSECs insert, as an alternative *in vitro* method for simulating liver sinusoid. The model allowed to maintain stable and functional cellular behaviours' and to study the crosstalk between cells. The modularity of our microfluidic platform suggests that other NPCs can be easily included to the model: Kupffer cells with LSECs insert and stellate cells in the biochip with hepatocytes. In addition to study of drug metabolism/toxicity and liver disease, the model offers the possibility of studying the complex cell-cell interactions which plays key role in liver injury and disease. However, studies using human primary cells, and including long-term cultures/exposures and the use of other chemical would be needed to expand the significance of this model.

ACKNOWLEDGEMENTS

This work and T. Messelmani PhD were funded by the ANR (Agence Nationale de la Recherche, France) through the MIMLIVEROnChip project (ANR-19-CE19-0020-01), and by a grant from the Contrat de Plan Etat-Région (CPER) Cancer 2015–2020.

CONFLICT OF INTEREST

HCS pharma is the BIOMIMESYS® Liver owner and is a partner of the ANR MimLiverOnChip. Co-authors Z. Souguir and N. Maubon are employees of HCS Pharma.

REFERENCES

1. **Messelmani, T., Morisseau, L., Sakai, Y., Legallais, C., Le Goff, A., Leclerc, E., and Jellali, R.:** Liver organ-on-chip models for toxicity studies and risk assessment. Lab Chip, **22**, 2423-2450 (2022).

2. **Son, Y. W., Choi, H. N., Che, J. H., Kang, B. C., and Yun, J. W.:** Advances in selecting appropriate non-rodent species for regulatory toxicology research: Policy, ethical, and experimental considerations. Regul. Toxicol. Pharmacol., **116**, 104757 (2020).

3. **Jellali, R., Jacques, S., Essaouiba, A., Gilard, F., Letourneur, F., Gakière, B., Legallais, C., Leclerc, E.:** Investigation of steatosis profiles induced by pesticides using liver organ-on-chip model and omics analysis. Food Chem. Toxicol., **152**, 112155 (2021).

4. **Ruoß, M., Vosough, M., Königsrainer, A., Nadalin, S., Wagner, S., Sajadian, S., Huber, D., Heydari, Z., Ehnert, S., Hengstler, J. G., and Nussler, A. K.:** Towards improved hepatocyte cultures: Progress and limitations. Food Chem. Toxicol., **138**, 111188 (2020).

5. **Soldatow, V. Y., Lecluyse, E. L., Griffith, L. G., and Rusyn, I.:** In vitro models for liver toxicity testing. Toxicol. Res., **2**, 23-39 (2013).

6. **Polidoro, M. A., Ferrari, E., Marzorati, S., Lleo, A., and Rasponi, M.:** Experimental liver models: From cell culture techniques to microfluidic organs-on-chip. Liver Int., **41**, 1744-1761 (2021).

7. **Bale, S. S., and Borenstein, J. T.:** Microfluidic Cell Culture Platforms to Capture Hepatic Physiology and Complex Cellular Interactions, Drug Metab. and Dispos., **46**, 1638-1646 (2018).

8. **LeCluyse, E. L., Witek, R. P., Andersen, M. E., and Powers, M. J.:** Organotypic liver culture models: meeting current challenges in toxicity testing. Crit. Rev. Toxicol., **42**, 501-548 (2012).

9. **Moradi, E., Jalili-Firoozinezhad, S., and Solati-Hashjin, M.:** Microfluidic organ-on-a-chip models of human liver tissue. Acta Biomater., **116**, 67-83 (2020).

10. **Beckwitt, C. H., Clark, A. M., Wheeler, S., Taylor, D. L., Stolz, D. B., Griffith, L., and Wells, A.:** Liver 'organ on a chip', Exp. Cell Res., **363**, 15-25 (2015).

11. **Bale, S. S., Geerts, S., Jindal, R., and Yarmush, M. L.:** Isolation and co-culture of rat parenchymal and non-parenchymal liver cells to evaluate cellular interactions and response, Sci. Rep., **6**, 25329 (2016).

12. **Milner, E., Ainsworth, M., McDonough, M., Stevens, B., Buehrer, J., Delzell, R., Wilson, C., and Barnhill, J.:** Emerging three-dimensional hepatic models in relation to traditional two-dimensional in vitro assays for evaluating drug metabolism and hepatoxicity. Med. Drug Discov., **8**, 100060 (2020).

13. **Panwar, A., Das, P., and Tan, L. P.:** 3D hepatic organoid-based advancements in liver tissue engineering. Bioengineering, **8**, 185 (2021).

14. **Merlier, F., Jellali, R., and Leclerc, E.:** Online monitoring of hepatic rat metabolism by coupling a liver biochip and a mass spectrometer. Analyst, **142**, 3747-3757 (2017).

15. **Lee, J. H., Ho, K. L., and Fan, S. K.:** Liver microsystems in vitro for drug response. J. Biomed. Sci., **26**, 88 (2019).

16. **Lee, S. Y., Kim, D., Lee, S. H., & Sung, J. H.:** Microtechnology-based in vitro models: Mimicking liver function and pathophysiology. APL Bioeng., **5**, 041505 (2021).

17. **Jellali, R., Bricks, T., Jacques, S., Fleury, M. J., Paullier, P., Merlier, F., Leclerc, E.:** Long-term human primary hepatocyte cultures in a microfluidic liver biochip show maintenance of mRNA levels and higher drug metabolism compared with Petri cultures. Biopharm. Drug Dispos., **37**, 264-275 (2016).

18. **Schepers, A., Li, C., Chhabra, A., Seney, B. T., & Bhatia, S.:** Engineering a perfusable 3D human liver platform from iPS cells. Lab Chip, **16**, 2644-2653 (2016).

19. **Yu, F., Deng, R., Hao Tong, W., Huan, L., Chan Way, N., IslamBadhan, A., Iliescu, C., and Yu, H.:** A perfusion incubator liver chip for 3D cell culture with application on chronic hepatotoxicity testing. Sci. Re., **7**, 14528 (2017).

20. **Yun, C., Kim, S. H., and Jung, Y. S.:** Current research trends in the application of in vitro three-dimensional models of liver cells. Pharmaceutics, **15**, 54 (2023).

21. **Fang, Y., and Eglen, R. M.:** Three-dimensional cell cultures in drug discovery and development. SLAS Discov., **22**, 456-472 (2017).

22. **Ortega-Ribera, M., Fernández-Iglesias, A., Illa, X., Moya, A., Molina, V., Maeso-Díaz, R., Fondevila, C., Peralta, C., Bosch, J., Villa, R., and Gracia-Sancho, J.:** Resemblance of the human liver sinusoid in a fluidic device with biomedical and pharmaceutical applications. Biotechnol. Bioeng., **115**, 2585-2594 (2018).

23. **Bale, S. S., Golberg, I., Jindal, R., McCarty, W. J., Luitje, M., Hegde, M., Bhushan, A., Usta, O. B., and Yarmush, M. L.:** Long-term coculture strategies for primary hepatocytes and liver sinusoidal endothelial cells, Tissue Eng. Part C Methods, **21**, 413-422 (2015).

24. **Xiao, W., Perry, G., Komori, K., and Sakai, Y.:** New physiologically-relevant liver tissue model based on hierarchically cocultured primary rat hepatocytes with liver endothelial cells. Integr. Biol., **7**, 1412-1422 (2015).

25. **Messelmani, T., Le Goff, A., Souguir, Z., Maes, V., Roudaut, M., Vandenhaute, E., Maubon, N., Legallais, C., Leclerc, E., and Jellali, R.:** Development of liver-on-chip integrating a hydroscaffold mimicking the liver's extracellular matrix. Bioengineering, **9**, 443 (2022).

26. **Bricks, T., Paullier, P., Legendre, A., Fleury, M. J., Zeller, P., Merlier, F., Anton, P. M., and Leclerc, E.:** Development of a new microfluidic platform integrating co-cultures of intestinal and liver cell lines. Toxicol. In Vitro, **28**, 885-895 (2014).

27. **Jellali, R., Paullier, P, Fleury, M. J., and Leclerc, E.:** Liver and kidney cells cultures in a new perfluoropolyether biochip. Sens. Actuators B Chem., **229**, 396-407 (2016).

28. **Souguir, Z., Vidal, G., Demange, E., and Louis, F.:** WO Pat., 2016166479A1 (2016).

622 29. **Livak, K. J., and Schmittgen, T. D.:** Analysis of relative gene expression data using real-
623 time quantitative PCR and the 2(-Delta Delta C(T)) method. Methods, **25**, 402-408 (2001).
624 30. **Bricks, T., Hamon, J., Fleury, M. J., Jellali, R., Merlier, F., Herpe, Y. E., Seyer, A.,**
625 **Regimbeau, J. M., Bois, F., and Leclerc, E.:** Investigation of omeprazole and phenacetin
626 first-pass metabolism in humans using a microscale bioreactor and pharmacokinetic models.
627 Biopharm. Drug Dispos., **36**, 275-293 (2015).
628 31. **Bhatia, S. N., Balis, U. J., Yarmush, M. L., and Toner, M.:** Effect of cell-cell interactions
629 in preservation of cellular phenotype: cocultivation of hepatocytes and nonparenchymal
630 cells, FASEB J., **13**, 1883-1900 (1999).
631 32. **Bhatia, S. N., Yarmush, M. L., and Toner, M.:** Controlling cell interactions by
632 micropatterning in co-cultures: hepatocytes and 3T3 fibroblasts. J. Biomed. Mater. Res., **34**,
633 189-199 (1997).
634 33. **van Grunsven L. A.:** 3D in vitro models of liver fibrosis. Adv. Drug Deliv. Rev., **121**, 133-
635 146 (2017).
636 34. **Lauschke, V. M., Shafagh, R. Z., Hendriks, D. F. G., and Ingelman-Sundberg, M.:** 3D
637 primary hepatocyte culture systems for analyses of liver diseases, drug metabolism, and
638 toxicity: emerging culture paradigms and applications. Biotechnol. J., **14**, e1800347 (2019).
639 35. **Du, Y., Li, N., Yang, H., Luo, C., Gong, Y., Tong, C., Gao, Y., Lü, S., and Long, M.:**
640 Mimicking liver sinusoidal structures and functions using a 3D-configured microfluidic
641 chip. Lab Chip, **17**, 782-794 (2017).
642 36. **Vis, M. A. M., Ito, K., and Hofmann, S.:** Impact of Culture Medium on Cellular
643 Interactions in in vitro Co-culture Systems. Front. Bioeng. Biotechnol., **8**, 911 (2020).
644 37. **Elvevold, K., Smedsrød, B., and Martinez, I.:** The liver sinusoidal endothelial cell: a cell
645 type of controversial and confusing identity. Am. J. Physiol. Gastrointest. Liver Physiol.,
646 **294**, G391-G400 (2008).

38. **Akbari, E., Spychalski, G. B., Rangharajan, K. K., Prakash, S., and Song, J. W.:** Flow dynamics control endothelial permeability in a microfluidic vessel bifurcation model, Lab Chip, **18**, 1084-1093 (2018).

39. **van Duinen, V., van den Heuvel, A., Trietsch, S. J., Lanz, H. L., van Gils, J. M., van Zonneveld, A. J., Vulto, P., and Hankemeier, T.:** 96 perfusable blood vessels to study vascular permeability in vitro. Sci. Rep., **7**, 18071 (2017).

40. **de Haan, W., Øie, C., Benkheil, M., Dheedene, W., Vinckier, S., Coppiello, G., Aranguren, X. L., Beerens, M., Jaekers, J., Topal, B., Verfaillie, C., Smedsrød, B., and Luttun, A.:** Unraveling the transcriptional determinants of liver sinusoidal endothelial cell specialization. Am. J. Physiol. Gastrointest. Liver Physiol., **318**, G803-G815 (2020).

41. **DeLeve L. D.:** Liver sinusoidal endothelial cells in hepatic fibrosis. Hepatology, **61**, 1740-1746 (2015).

42. **Guguen-Guillouzo, C., and Guillouzo, A.:** General review on in vitro hepatocyte models and their applications. Methods Mol. Biol., **640**, 1-40 (2010).

43. **Donato, M. T., Tolosa, L., and Gómez-Lechón, M. J.:** Culture and functional characterization of human hepatoma HepG2 Cells. Methods Mol. Biol., **1250**, 77-93 (2015).

44. **Thomann, S., Weiler, S. M. E., Marquard, S., Rose, F., Ball, C. R., Tóth, M., Wei, T., Sticht, C., Fritzsche, S., Roessler, S., and other 10 authors:** YAP orchestrates heterotypic endothelial cell communication via HGF/c-MET signaling in liver tumorigenesis. Cancer Res., **80**, 5502-5514 (2020).

45. **Lee, D., Park, J. S., Kim, D., and Hong, H. S.:** Substance P hinders bile acid-induced hepatocellular injury by modulating oxidative stress and inflammation. Antioxidants, **11**, 920 (2022).

46. **Behrends, V., Giskeødegård, G. F., Bravo-Santano, N., Letek, M., and Keun, H. C.:** Acetaminophen cytotoxicity in HepG2 cells is associated with a decoupling of glycolysis

672 from the TCA cycle, loss of NADPH production, and suppression of anabolism. Arch.
673 Toxicol., **93**, 341-353 (2019).
674 47. **Leclerc, E., Hamon, J., Claude, I., Jellali, R., Naudot, M., and Bois, F.:** Investigation of
675 acetaminophen toxicity in HepG2/C3a microscale cultures using a system biology model of
676 glutathione depletion. Cell Biol. Toxicol., **31**, 173-185 (2015).
677 48. **Prot, J. M., Briffaut, A. S., Letourneur, F., Chafey, P., Merlier, F., Grandvalet, Y.,**
678 **Legallais, C., and Leclerc, E.:** Integrated proteomic and transcriptomic investigation of the
679 acetaminophen toxicity in liver microfluidic biochip. PloS one, **6**, e21268 (2011).
680 49. **Prot, J. M., Bunescu, A., Elena-Herrmann, B., Aninat, C., Snouber, L. C., Griscom,**
681 **L., Razan, F., Bois, F. Y., Legallais, C., Brochot, C., Corlu, A., Dumas, M. E., and**
682 **Leclerc, E.:** Predictive toxicology using systemic biology and liver microfluidic "on chip"
683 approaches: application to acetaminophen injury. Toxicol. Appl. Pharmacol., **259**, 270-280
684 (2012).
685 50. **Mazaleuskaya, L. L., Sangkuhl, K., Thorn, C. F., FitzGerald, G. A., Altman, R. B.,**
686 **and Klein, T. E.:** PharmGKB summary: pathways of acetaminophen metabolism at the
687 therapeutic versus toxic doses. Pharmacogenet. Genomics, **25**, 416-426 (2015).
688 51. **Badmann, A., Langsch, S., Keogh, A., Brunner, T., Kaufmann, T., and Corazza, N.:**
689 TRAIL enhances paracetamol-induced liver sinusoidal endothelial cell death in a Bim- and
690 Bid-dependent manner, Cell Death Dis., **3**, e447 (2012).
691 52. **Holt, M. P., Yin, H., and Ju, C.:** Exacerbation of acetaminophen-induced disturbances of
692 liver sinusoidal endothelial cells in the absence of Kupffer cells in mice. Toxicol. Lett., **194**,
693 34-41 (2010).
694 53. **González, L. T., Minsky, N. W., Espinosa, L. E., Aranda, R. S., Meseguer, J. P., and**
695 **Pérez, P. C.:** In vitro assessment of hepatoprotective agents against damage induced by
696 acetaminophen and CCl4. BMC Complement. Altern. Med., **17**, 39 (2017).

54. **Odeyemi, S., and Dewar, J.:** Repression of acetaminophen-induced hepatotoxicity in HepG2 cells by polyphenolic compounds from Lauridia tetragona (L.f.) R.H. Archer. Molecules, **24**, 2118 (2019).

55. **Kang, Y. B., Sodunke, T. R., Lamontagne, J., Cirillo, J., Rajiv, C., Bouchard, M. J., and Noh, M.:** Liver sinusoid on a chip: Long-term layered co-culture of primary rat hepatocytes and endothelial cells in microfluidic platforms. Biotechnol. Bioeng., **112**, 2571-2582 (2015).

56. **Prodanov, L., Jindal, R., Bale, S. S., Hegde, M., McCarty, W. J., Golberg, I., Bhushan, A., Yarmush, M. L., and Usta, O. B.:** Long-term maintenance of a microfluidic 3D human liver sinusoid. Biotechnol. Bioeng., **113**, 241-246 (2016).

57. **Ma, L. D., Wang, Y. T., Wang, J. R., Wu, J. L., Meng, X. S., Hu, P., Mu, X., Liang, Q. L., and Luo, G. A.:** Design and fabrication of a liver-on-a-chip platform for convenient, highly efficient, and safe in situ perfusion culture of 3D hepatic spheroids. Lab Chip, **18**, 2547-2562 (2018).

720 **Fig.1.** (A) Pictures and schematic image showing the design and principle of the IIDMP
721 coculture platform; (B) experimental procedures for SK-HEP-1 and HepG2/C3A monoculture
722 and coculture.
723 **Fig.2**. Effect of culture medium composition on SK-HEP-1 and HepG2/C3a cells cultured in
724 static inserts and 6-well plate, respectively. (A) phase contrast microscopy images of SK-HEP-
725 1 exhibiting similar morphologies after 7 days of culture in EGM-2/MEM (75%/25%) and
726 EGM-2/MEM (25%/75%) mixtures (magnification x10); (B) gene expression of several LSECs
727 markers in SK-HEP-1 cultured in EGM-2/MEM (75%/25%) and EGM-2/MEM (25%/75%)
728 mixtures: CLEC4M and VCAM1 are downregulated in EGM-2/MEM (25%/75%) mixtures (*
729 $P < 0.05$, $n = 3$); (C and D) HepG2/C3a cell with similar morphologies and albumin secretion
730 ($n = 6$) after 4 days of culture in MEM and EGM-2/MEM (25%/75%) mixture media.
731 **Fig.3.** Characterisation of the SK-HEP-1 endothelial barrier. (A) vimentin, actin, and nuclei
732 staining of the SK-HEP-1 cells after 8 days of culture on inserts; (B) PECAM-1, stabilin-2, and
733 nuclei staining at Day 8; (C) apparent permeability to Lucifer Yellow, measured between day
734 4 and day 15: SK-HEP-1 barrier reaches its stable permeability from day 8 ($35\text{-}40 \times 10^{-15} \pm 8 \times$
735 10^{-15} m/s), * $P < 0.05$ ($n = 6$); (D) diffusion of FITC-dextran (4, 70 and 150 kDa) through the
736 SK-HEP-1 confluent barrier (8 days of culture) and insert without cells ($n = 6$): the diffusion
737 decreases in the presence of the SK-HEP-1 barrier and with increasing dextran molecular
738 weight.
739 **Fig.4.** Characterisation of the SK-HEP-1 endothelial barrier in dynamic monoculture and
740 coculture (8 days of maturation followed by 2 days in the IIDMP platform). (A) vimentin, actin,
741 and nuclei staining; (B) PECAM-1, stabilin-2 and nuclei staining.
742 **Fig.5.** Comparison of the SK-HEP-1 barrier in dynamic monoculture and coculture. (A) gene
743 expression of LSECs markers: KDR and CLEC4M are down- and upregulated, respectively in

744 dynamic coculture, * P < 0.05 (n = 3); (B) FITC-dextran 4 kDa diffusion through SK-HEP-1
745 barriers in dynamic monoculture and coculture (n = 6).
746 **Fig.6.** Characterisation of HepG2/C3a cells cultured in the biochip, in monoculture, and
747 coculture with the SK-HEP-1 endothelial barrier. (A) cell morphology after seeding, 24 h of
748 adhesion in static conditions, 48 h of dynamic monoculture, and 48 h of dynamic coculture in
749 the presence of SK-HEP-1; (B) no significant difference in albumin secreted by HepG2/C3a
750 cells during the 48 h of dynamic monoculture/coculture with SK-HEP-1 (n = 6); (C) urea
751 quantification showing downregulation in the coculture conditions, * P < 0.05 (n = 6); (D)
752 similar gene expression of HepG2/C3a markers in monocultures and cocultures (n = 3).
753 **Fig.7.** Characterisation of the SK-HEP-1 endothelial barrier exposed to APAP in dynamic
754 monoculture and coculture, 8 days of maturation followed by 2 days in the IIDMP platform
755 with APAP exposure. (A) vimentin, actin, and nuclei staining; (B) PECAM-1, stabilin-2 and
756 nuclei staining. The Actin organization and the expression levels of PECAM-1 and stabilin-2
757 (low) appear affected by APAP exposure (in comparison with monoculture and coculture
758 without APAP in Fig.4).
759 **Fig.8.** Characterisation of monocultures and cocultures with and without APAP treatment. (A)
760 mRNA ratio (APAP+/APAP-) of selected markers in SK-HEP-1 monoculture and coculture
761 (comparison APAP+ versus APAP-): APAP exposure leads to MRC1 upregulation and KDR,
762 CLEC4M downregulation in monoculture, and KDR upregulation in coculture, * P < 0.05 (n =
763 3); (B) mRNA ratio (APAP+/APAP-) of selected markers in HepG2/C3a monoculture and
764 coculture (comparison APAP+ versus APAP-): only UGT2B7 is downregulated in coculture
765 exposed to APAP, * P < 0.05 (n = 3); (C) ratio (APAP+/APAP-) of albumin and urea secreted
766 by HepG2/C3a monoculture and coculture; urea secretion decreases in monoculture and
767 coculture treated with APAP, * P < 0.05 (n = 6); (D) ratio of APAP recovered at the end of the
768 experiments for HepG2/C3a monoculture, SK-HEP-1 monoculture and coculture: SK-HEP-1

769 monoculture do not metabolize APAP , * $P < 0.05$ ($n = 6$); (E) expression of inflammatory
770 genes in SK-HEP-1 monoculture and coculture, with and without APAP, showing the
771 upregulation of TNFα in coculture exposed to APAP, * $P < 0.05$ ($n = 3$); (F) expression of
772 inflammatory genes in HepG2/C3a monoculture and coculture, with and without APAP: the
773 exposure to APAP decreases the expression of TNFα in coculture, * $P < 0.05$ ($n = 3$); (G) IL-6
774 secreted in different culture conditions.
775

Figure 1

Click here to access/download;Figure;Fig.1.tif

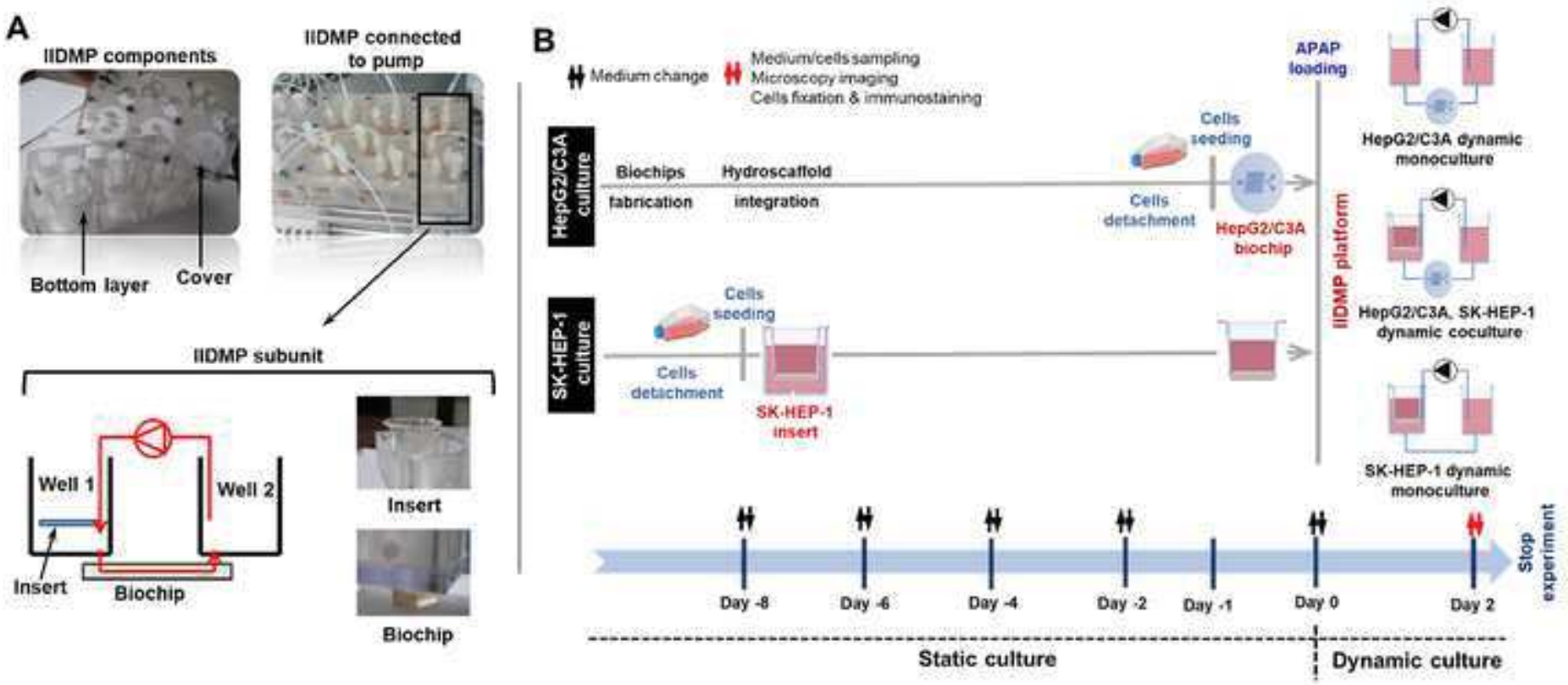

Figure 2

Click here to access/download;Figure;Fig.2.tif

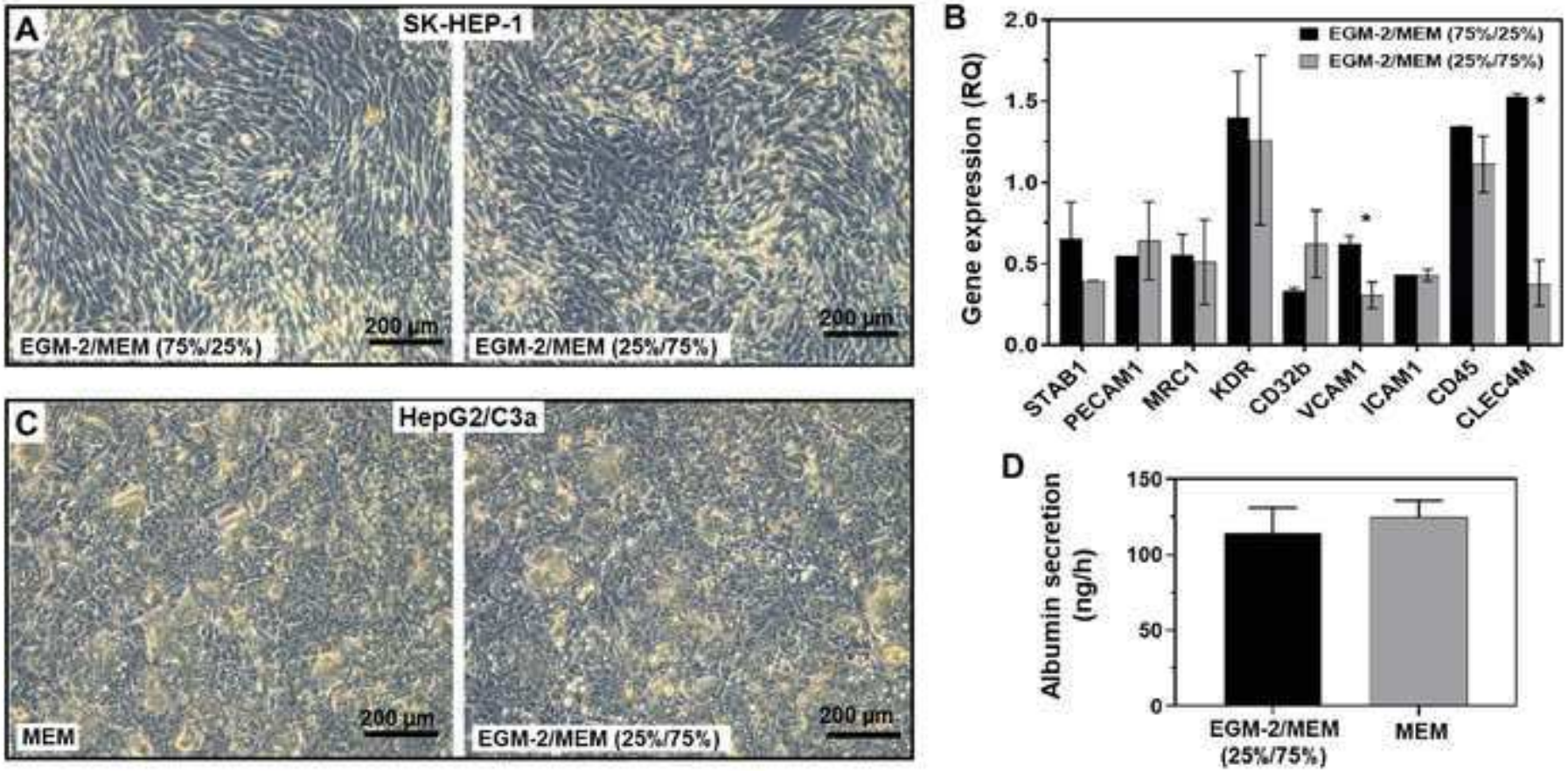

Figure 3

Click here to access/download;Figure;Fig.3.tif

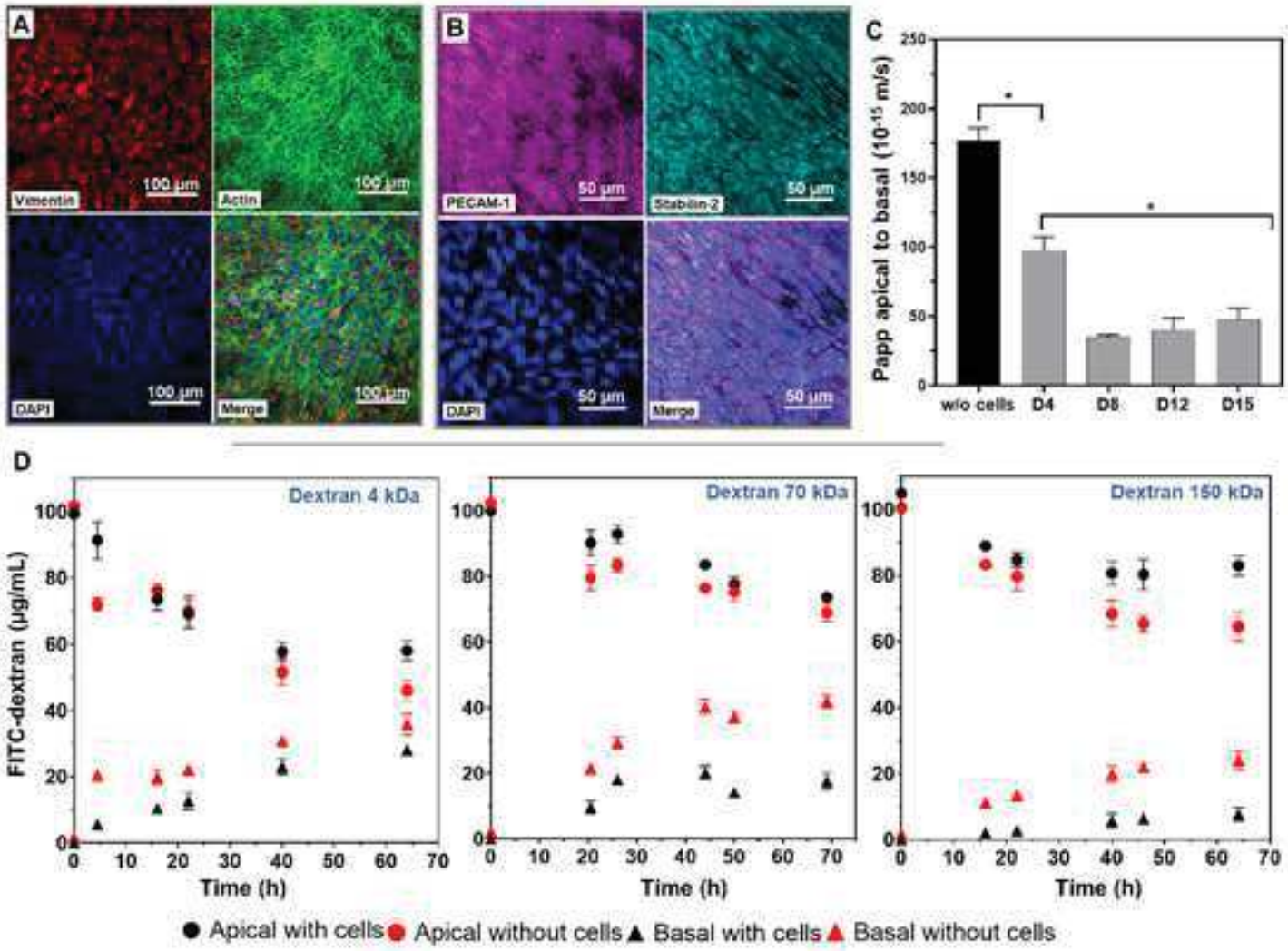

Figure 4

Click here to access/download;Figure;Fig.4.tif

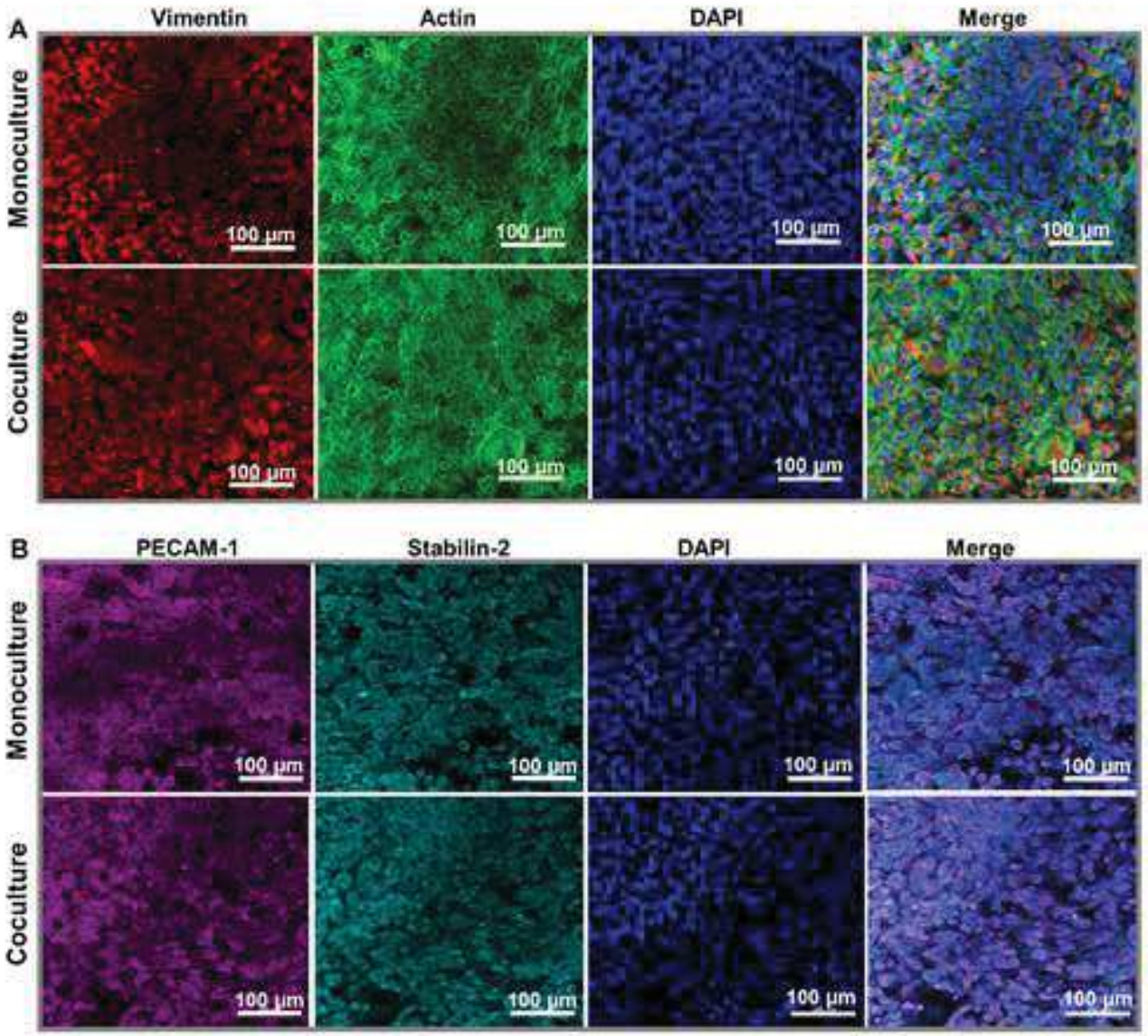

Figure 5

Click here to access/download;Figure;Fig.5.tif

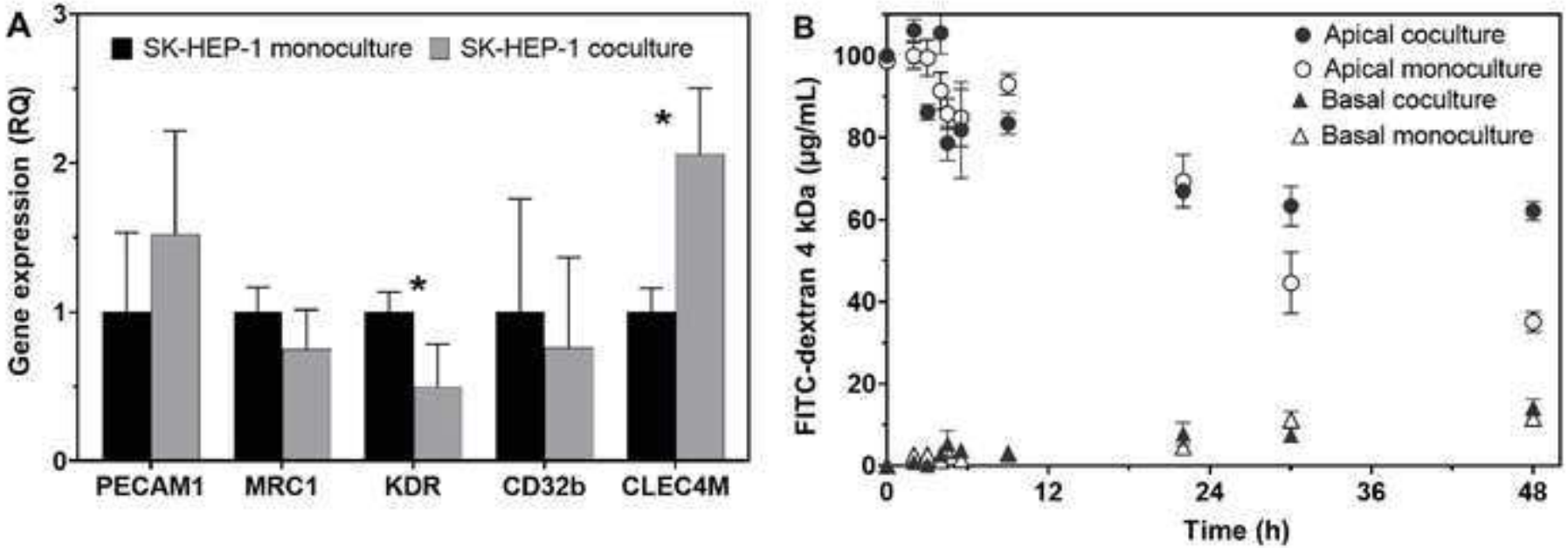

Figure 6

Click here to access/download;Figure;Fig.6.tif

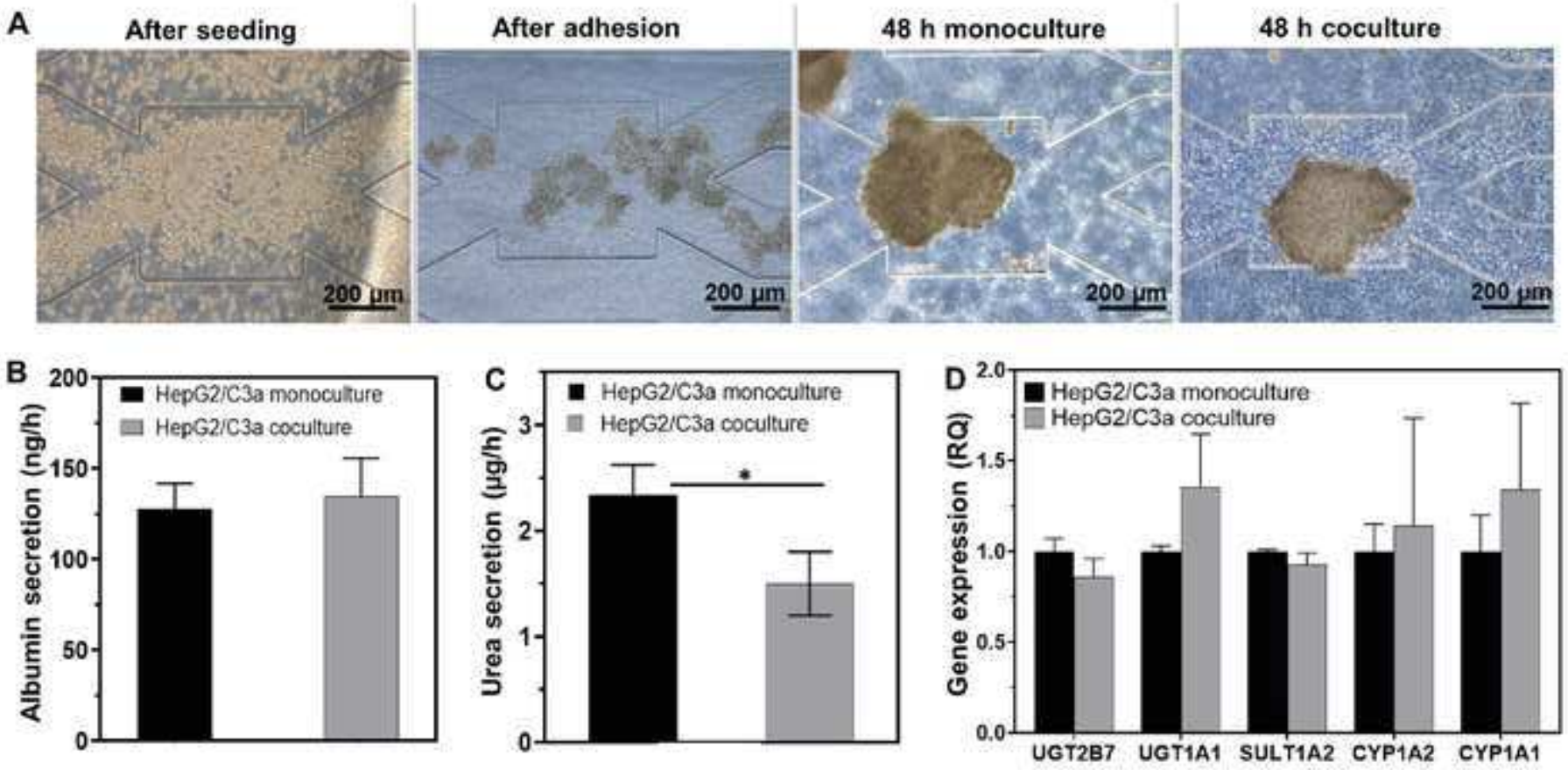

Figure 7

Click here to access/download;Figure;Fig.7.tif

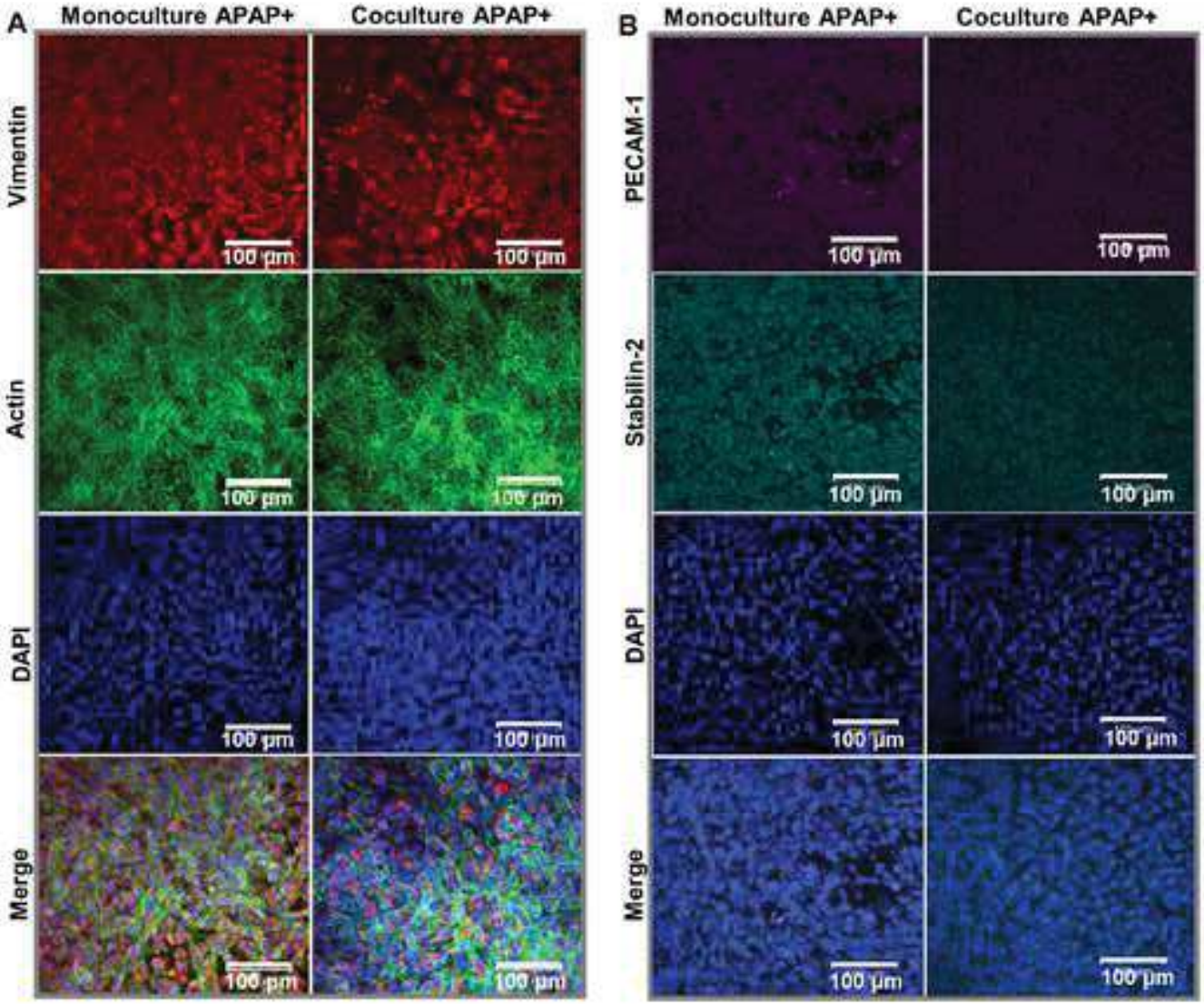

Figure 8

Click here to access/download;Figure;Fig.8.tif

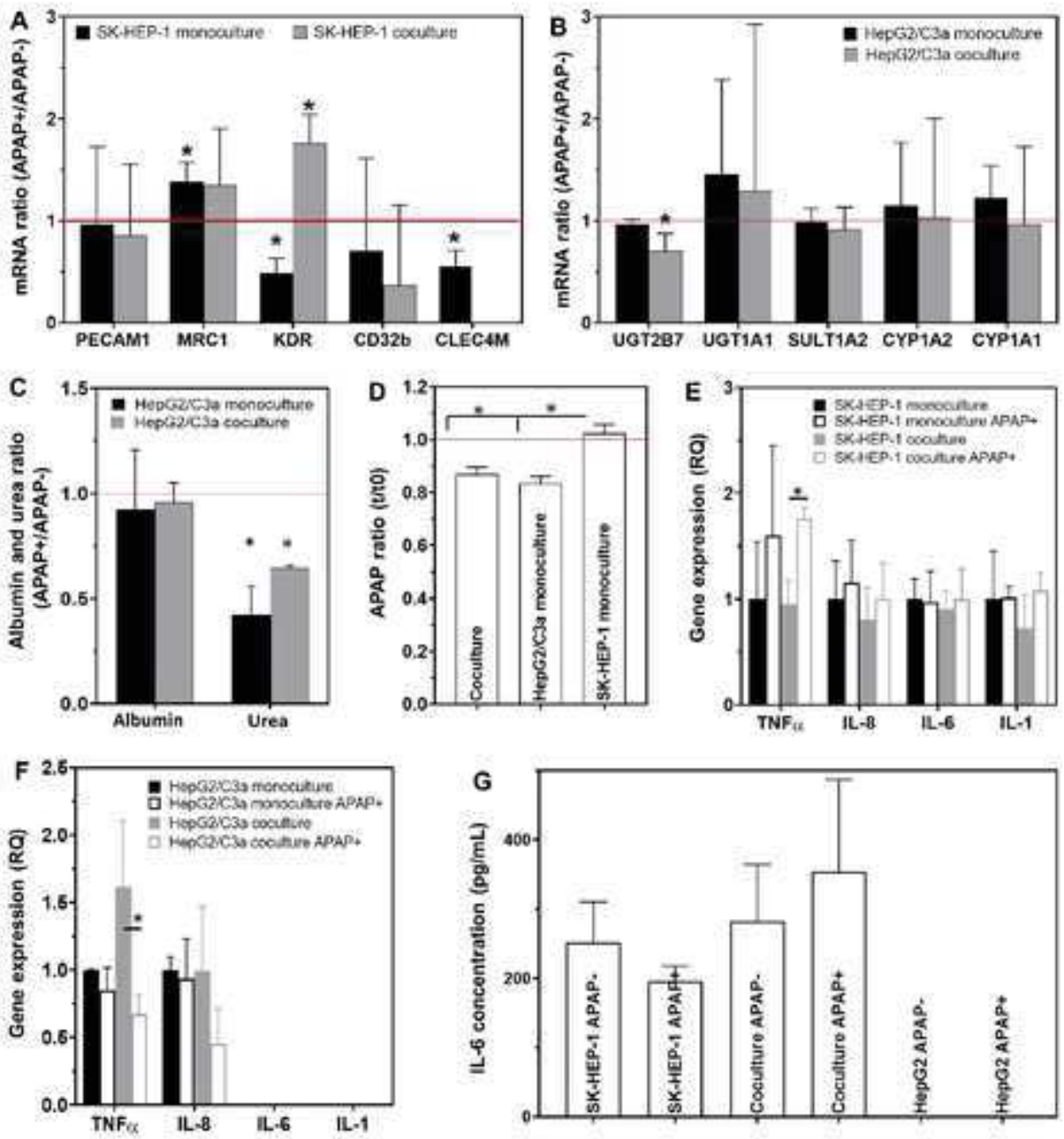

Coculture model of a liver sinusoidal endothelial cell barrier and HepG2/C3a spheroids-on-chip in an advanced fluidic platform

Taha Messelmani [1], Anne Le Goff [1], Fabrice Soncin [2,3], Zied Souguir [4], Franck Merlier [5], Nathalie Maubon [4], Cécile Legallais [1], Eric Leclerc [1,3], Rachid Jellali[1]*

[1] *Université de Technologie de Compiègne, CNRS, Biomechanics and Bioengineering, Centre de recherche Royallieu-CS 60319 -60203 Compiègne Cedex, France*

[2] *CNRS/IIS/Centre Oscar Lambret/Lille University SMMiL-E Project, CNRS Délégation Hauts-de-France, 43 Avenue le Corbusier, 59800 Lille, France*

[3] *CNRS, IRL2820, Laboratory for Integrated Micro Mechatronic Systems, Institute of Industrial Science, University of Tokyo, 4-6-1 Komaba, Meguro-ku, Tokyo 153-8505, Japan*

[4] *HCS Pharma, 250 rue Salvador Allende, Biocentre Fleming Bâtiment A, 59120 Loos, France*

[5] *Université de Technologie de Compiègne, UPJV, CNRS, Enzyme and Cell Engineering, Centre de Recherche Royallieu, Cedex CS 60319, 60203 Compiègne, France*

Corresponding authors: Rachid Jellali (rachid.jellali@utc.fr)

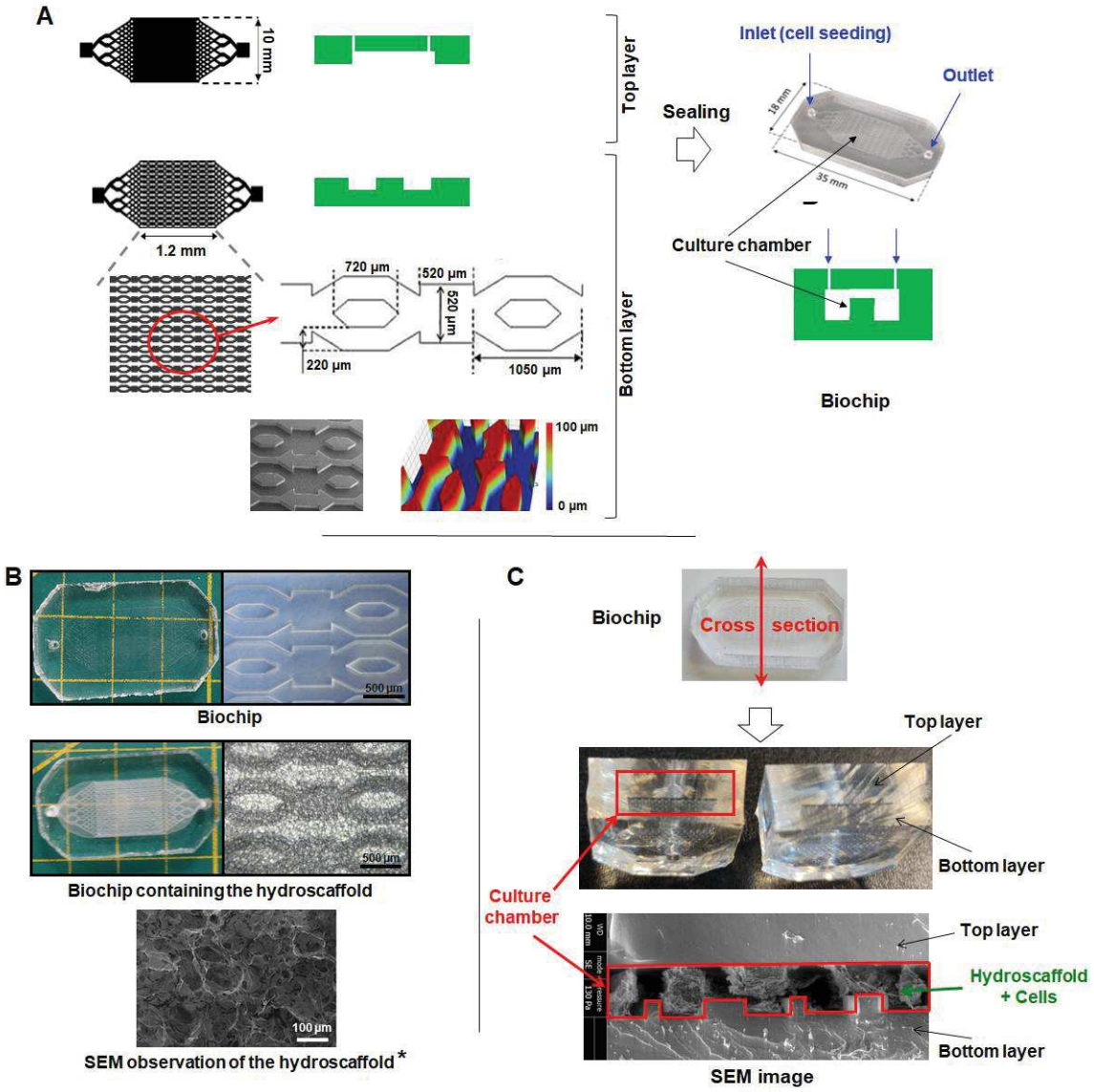

Fig.S1. Specifications of the biochip used for HepG2/C3a cultures. (A) biochip design and dimensions; (B) characterisation of the biochip with and without the hydroscaffold: images, optical microscope observations of the biochips (magnification x5) and SEM image of the hydroscaffold (* data from Messelmani et al., 2022 **(25)**); (C) image and SEM observation of biochip cross section showing the culture chamber containing the hydroscaffold and cells. Scanning electron microscopy (SEM) analysis was taken using an XL30-ESEM FEG (Philips, Eindhoven, The Netherlands), with samples (cells + hydroscaffold) fixed in paraformaldehyde 4%.

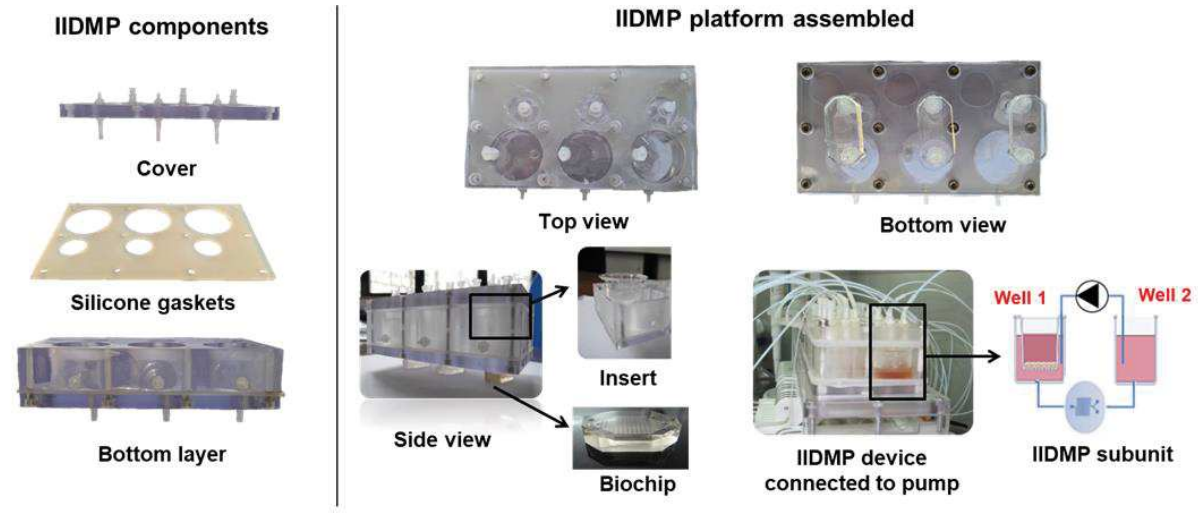

Fig.S2. Specifications and principle of the IIDMP platform.

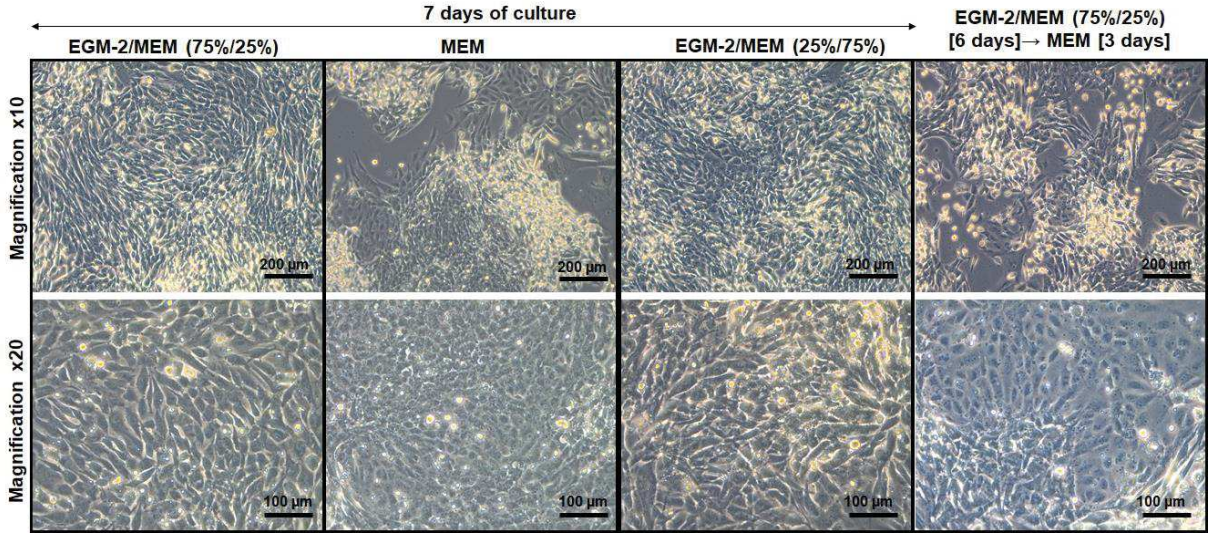

Fig.S3. Phase contrast microscopy images of SK-HEP-1 cells cultured on static inserts in different culture media mixtures. Among the tested conditions, only the mixture EGM-2/MEM (25%/75%) allows the formation of confluent barrier similar to barrier formed by SK-HEP-1 cells cultured in their original medium (SK-HEP-1 cells are routinely cultured in EGM-2/MEM (75%/25%) mixture).

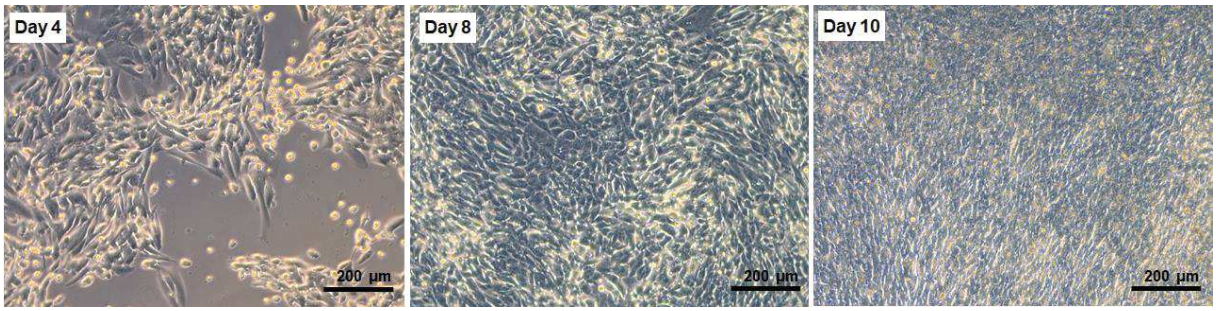

Fig.S4. Phase contrast microscopy images (magnification x10) showing the growing of the SK-HEP-1 cell layer between day 4 and 10. The cells were cultured on static inserts.

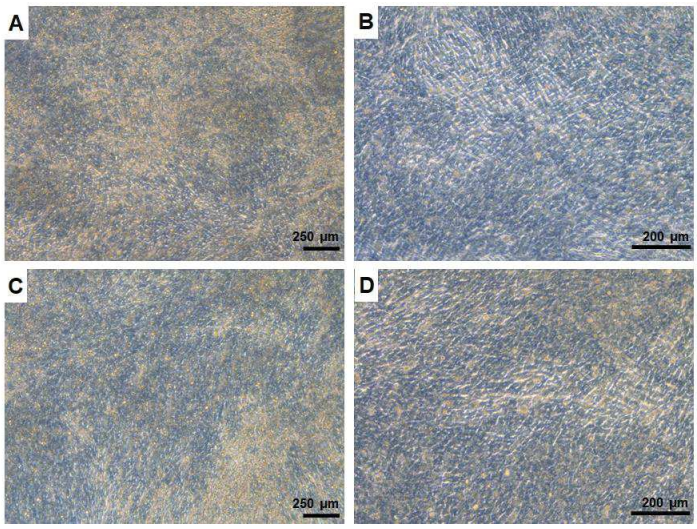

Fig.S5. Phase contrast microscopy images of SK-HEP-1 cells monoculture and coculture after 10 days of culture: 8 days of maturation in static inserts and 2 days of dynamic culture in IIDMP platform (A and C: magnification x5; B and D: magnification x10). No significant difference was observed between the SK-HEP-1 monoculture and coculture (with HepG2/C3a).

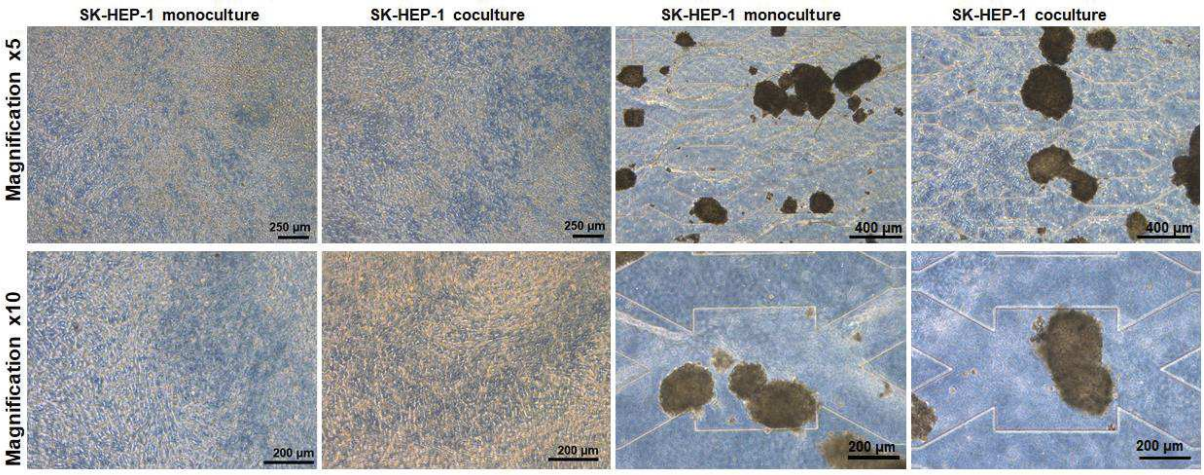

Fig.S6. Phase contrast microscopy images of SK-HEP-1 and HepG2/C3a cells monoculture and coculture after exposure to APAP for 2 days (dynamic culture in IIDMP platform). The morphological features of HepG2/C3a spheroids and SK-HEP-1 barrier remain unchanged after exposure to APAP (in monoculture and coculture).

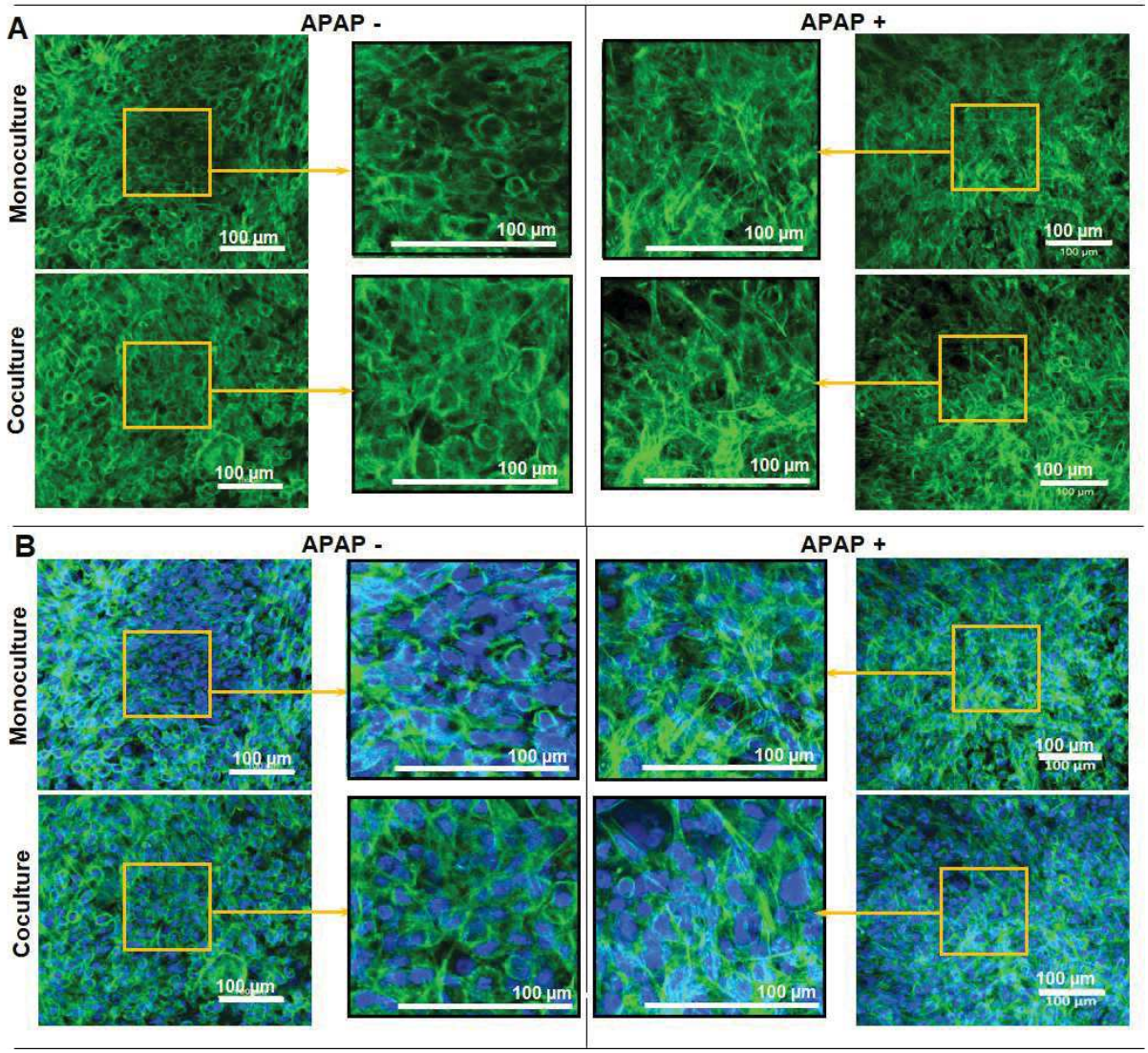

Fig.S7. Characterisation of the SK-HEP-1 endothelial barrier exposed in dynamic monoculture and coculture: 8 days of maturation followed by 2 days in the IIDMP platform with and without APAP exposure. (A) actin staining; (B) actin and nuclei staining (merge). The Actin organization appear affected by APAP exposure.

Table S1. TaqMan probes used for RTqPCR assays.

Gene	Probe ID	Fluorophore
B2M	Human B2M (beta-2-microglobulin) Endogenous Control	VIC/MGB probe, primer limited
STAB1	Hs01109068_m1	FAM/MGB
PECAM1	Hs01065279_m1	FAM/MGB
MRC1	Hs00267207_m1	FAM/MGB
KDR	Hs00911700_m1	FAM/MGB
CD32b	Hs01634996_s1	FAM/MGB
VCAM1	Hs01003372_m1	FAM/MGB
ICAM1	Hs00164932_m1	FAM/MGB
CD45	Hs04189704_m1	FAM/MGB
CLEC4M	Hs03805885_g1	FAM/MGB
UGT2B7	Hs00426592_m 1	FAM/MGB
UGT1A1	Hs02511055_s1	FAM/MGB
SULT1A2	Hs02340929_g1	FAM/MGB
CYP1A2	Hs00167927 _m1	FAM/MGB
CYP1A1	Hs01054796_g1	FAM/MGB
TNFα	Hs01113624_g1	FAM/MGB
IL-1	Hs01555410_m1	FAM/MGB
IL-6	Hs00985639_m1	FAM/MGB
IL-8/ CXCL8	Hs00174103_m1	FAM/MGB